

AMERICAN UNIVERSITY OF BEIRUT

A POWER REROUTING STRATEGY IN
ELECTRICAL MICROGRIDS UNDER
POWER ELECTRONICS FAULTS

by

ABDALLAH HUSSEIN NASSER ELDEEN

A thesis

submitted in partial fulfillment of the requirements
for the degree of Master of Engineering
to the Department of Electrical and Computer Engineering
of Maroun Semaan Faculty of Engineering and Architecture
at the American University of Beirut

Beirut, Lebanon
February 2021

AMERICAN UNIVERSITY OF BEIRUT

A POWER REROUTING STRATEGY IN
ELECTRICAL MICROGRIDS UNDER
POWER ELECTRONICS FAULTS

by

ABDALLAH HUSSEIN NASSER ELDEEN

Approved by:



Dr. Ali Bazzi, Associate Professor
Electrical and Computer Engineering

Advisor

Dr. Riad Chedid, Professor
Electrical and Computer Engineering



Member of Committee

Dr. Sami Karaki, Professor
Electrical and Computer Engineering

Member of Committee

Date of thesis defense: February 19, 2021

AMERICAN UNIVERSITY OF BEIRUT

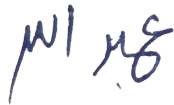
THESIS, DISSERTATION, PROJECT RELEASE FORM

Student Name: Nasser Eldeen Abdallah Hussein
Last First Middle

Master's Thesis Master's Project Doctoral Dissertation

I authorize the American University of Beirut to: (a) reproduce hard or electronic copies of my thesis, dissertation, or project; (b) include such copies in the archives and digital repositories of the University; and (c) make freely available such copies to third parties for research or educational purposes.

I authorize the American University of Beirut, to: (a) reproduce hard or electronic copies of it; (b) include such copies in the archives and digital repositories of the University; and (c) make freely available such copies to third parties for research or educational purposes after: **One ___ year from the date of submission of my thesis, dissertation or project.**
Two ___ years from the date of submission of my thesis , dissertation or project.
Three ___ years from the date of submission of my thesis , dissertation or project.



Signature

28/2/2021

Date

Acknowledgements

First of all, I would like to thank God for all his mercies during my whole research work which would not have succeeded without his aid.

Then I would like to express my sincere gratitude and deep greetings to my advisor, professor Ali M. Bazzi. He was a real supporter who provided me with a professional and healthy research environment. I benefited greatly from all our technical discussions to accomplish my work.

Finally, I would like to thank my family for their encouragement and being beside me, especially my brother Ali who always pushed me forward during my research journey.

An Abstract of the Thesis of

Abdallah Hussein Nasser Eldeen for Master of Engineering
Major: Electrical and Computer Engineering

Title: A Power Rerouting Strategy in Electrical Microgrids Under Power Electronics Faults

Due to rising environmental concerns and limited fossil fuels, clean and renewable resources are being used in power generation. Microgrids are used to connect these energy resources to local demand using power electronics interfaces. Power electronics faults at the inverter stage are critical issues that limit a microgrid's performance. In the literature, many techniques for fault-tolerant inverters were proposed. In this thesis, a system-level fault-tolerant method is proposed for microgrid inverters. It is applied by adding a controlled bidirectional switch between parallel inverters to allow for rerouting power during faults. The method is simulated and verified on PV inverters as well as grid-interfaced batteries. Results show that it is possible to recover significant amounts of curtailed power lost from distributed energy resources when their power electronics interfaces suffer from faults. An experimental prototype also verifies the methodology.

Contents

Acknowledgements	v
Abstract	vi
Abbreviations	xi
1 Introduction	1
1.1 Problem Definition	2
2 Literature Review	3
2.1 State of the Art in Microgrids	3
2.1.1 Microgrid components	3
2.1.2 Microgrid Operation	4
2.1.3 Microgrid Control	5
2.1.3.1 Internal control loop	6
2.1.3.2 Primary control	6
2.1.3.3 Secondary control	7
2.1.3.4 Tertiary control	7
2.2 Fault-Tolerant and Multi-Parallel Power Converters	7
2.2.1 Fault Tolerance Levels of Power Converters	7
2.2.2 Parallel Multi-inverters in a Microgrid	10
3 Proposed Solution for Retrieving Lost Power	11
3.1 Bidirectional switch	11
3.2 Fault Scenario	11
4 Microgrid and Algorithm simulation	14
4.1 Application in PV Systems	14
4.1.1 Normal Operation	15
4.1.2 Fault Operation	19
4.1.2.1 Fault at t=10s	19
4.1.2.2 Fault at t=50s	22
4.1.3 Advantages	25
4.1.4 Operation Under Realistic Solar Irradiance	26

4.2	Application in Battery Systems	28
4.2.1	Normal Operation	29
4.2.1.1	Active Power Generation	29
4.2.1.2	Active and Reactive Power Generation	33
4.2.2	Fault Operation	35
4.2.3	Advantages	39
4.3	Overall Microgrid	39
4.3.1	Microgrid operation with no load	40
4.3.2	Microgrid operation with 500 KW load	41
4.3.3	Microgrid operation with 1000 KW load	42
4.3.4	Microgrid operation under fault with 500 KW load	43
5	Experimental Results	44
6	Conclusion and Future Work	46

List of Figures

2.1	Basic Microgrid architecture with an MGCC [1]	4
2.2	Hierarchical control of a microgrid [2]	6
2.3	Voltage and frequency versus active and reactive power	7
2.4	Fault tolerant methodology chart	8
2.5	Fault tolerant inverters topologies. (a) Switch level. (b) Leg level. (c) Module level. (d) System level.	9
3.1	Bidirectional switch addition	12
3.2	Bidirectional switch realizations	12
3.3	Fault scenario	13
3.4	Switching algorithm flow chart	13
4.1	MATLAB Simulink schematic of grid connected solar arrays	14
4.2	Control blocks of the inverters	15
4.3	Three phase grid voltage	15
4.4	Bidirectional switch state in normal operation	16
4.5	Solar arrays DC voltage in normal operation	16
4.6	Power injected to grid in normal operation	17
4.7	Power output of inverters in normal operation	17
4.8	Phase 'a' RMS current injected to grid in normal operation	18
4.9	Phase 'a' RMS output currents of inverters in normal operation	18
4.10	Bidirectional switch state (fault at 10s)	19
4.11	Solar arrays DC voltage (fault at 10s)	20
4.12	Power injected to grid (fault at 10s)	20
4.13	Power output of inverters 1 (healthy) and 2 (faulty) (fault at 10s)	21
4.14	Phase 'a' RMS current injected to grid (fault at 10s)	21
4.15	Phase 'a' RMS output currents of inverters 1 (healthy) and 2 (faulty) (fault at 10s)	22
4.16	Bidirectional switch state (fault at 50s)	22
4.17	Solar arrays DC voltage (fault at 50s)	23
4.18	Power injected to grid (fault at 50s)	23
4.19	Power output of inverters 1 (healthy) and 2 (faulty) (fault at 50s)	24
4.20	Phase 'a' RMS current injected to grid (fault at 50s)	24

4.21	Phase 'a' RMS output currents of inverters 1 (healthy) and 2 (faulty) (fault at 50s)	25
4.22	Solar irradiance in Beirut at 5:00 am till 5:10	26
4.23	Power injected to grid under realistic solar irradiance	27
4.24	Power output for inverters under realistic solar irradiance	27
4.25	MATLAB Simulink schematic of grid connected storage banks	28
4.26	Control blocks of the inverters	28
4.27	Three phase grid voltage	29
4.28	Bidirectional switch state in normal operation	30
4.29	Power injected to grid in normal operation	30
4.30	Power output of inverters in normal operation	31
4.31	Storage banks state of charge in normal operation	31
4.32	Phase 'a' RMS current injected to grid in normal operation	32
4.33	Phase 'a' RMS output currents of inverters in normal operation	32
4.34	Power injected to grid in normal operation2	33
4.35	Power output of inverters in normal operation2	33
4.36	Storage banks state of charge in normal operation2	34
4.37	Phase 'a' RMS current injected to grid in normal operation2	34
4.38	Phase 'a' RMS output currents of inverters in normal operation2	35
4.39	Bidirectional switch state (fault at 30s)	36
4.40	Power injected to grid (fault at 30s)	36
4.41	Power output of inverters 1 (healthy) and 2 (faulty) (fault at 30s)	37
4.42	Storage banks state of charge (fault at 30s)	37
4.43	Phase 'a' RMS current injected to grid (fault at 30s)	38
4.44	Phase 'a' RMS output currents of inverters 1 (healthy) and 2 (faulty) (fault at 30s)	38
4.45	MATLAB Simulink schematic of proposed microgrid	39
4.46	Power flow in microgrid components at no load	40
4.47	Power flow in microgrid components at 500 KW load	41
4.48	Power flow in microgrid components at 1000 KW load	42
4.49	Power flow in microgrid components at 500 KW load under fault	43
5.1	Experimental setup	44
5.2	Experimental results before the fault is emulated in inverter 1	45
5.3	Experimental results after t_1 when inverter 1 is taken offline	45
5.4	Experimental results after t_2	45

Abbreviations

PCC	Point Of Common Coupling
DER	Distributed Energy Resource
MGCC	Microgrid Central Controller
DG	Distributed Generator
ESS	Energy Storage System
PV	Photo-Voltaic
UPS	Uninterruptible Power Supply
MPPT	Maximum Power Point Tracking
V_{oc}	Open Circuit Voltage
SoC	State of Charge

Chapter 1

Introduction

Today's societies depend on secure sources of energy [3]. Aging of the current infrastructure challenges the reliability of the power supply, and new electricity grids should consider both economical and environmental aspects of an energy system. Motivated by these two conditions, there is a global trend to switch towards clean energy sources such as photovoltaic (PV) panels, fuel cells and wind turbines [4, 5]. These resources are considered as distributed generation. To get benefit from distributed generation, the notion of microgrid evolved. As defined by the US Department of Energy, "The Microgrid is a group of interconnected loads and distributed energy resources with clearly defined electrical boundaries that acts as a single controllable entity with respect to the grid and can connect and disconnect from the grid to enable it to operate in both grid-connected or island modes" [6]. Therefore, a microgrid is not just a storage unit or backup generator. It is similar to a small-scale power system that can generate, distribute and regulate the flow of energy. Microgrids are becoming more common due to the significant drop in their main components' prices. For example, the price of silicon PV cell dropped from 76.67 \$/watt in 1977 to 0.3 \$/watt in 2015 [7].

Microgrids require power electronic interfaces such as DC/AC or AC/DC/AC converters to interface the electrical system with the distributed generation. Electrolytic capacitors and power switching devices in such converters are the most vulnerable components that challenge the reliability of a converter. Any fault that may occur in any component would interrupt the operation of the converter and thus major chunks of the microgrid [8].

1.1 Problem Definition

When a fault occurs at any inverter in the microgrid, the latter loses the power generated from the corresponding generator, such as PV array or battery. Thus the total energy circulating in the system will be reduced. In this thesis, a new method is proposed to minimize the curtailed power of a faulty inverter by rerouting it to another healthy inverter in the microgrid, via a controlled bidirectional switch between the inputs of both inverters.

Chapter 2

Literature Review

The objective of this literature survey is to give a general overview about some important concepts related to the thesis work. First, an overview about the microgrid notion, operation and control, is given. Then, fault tolerance techniques and controlling parallel inverters are presented, as they relate to the proposed new method.

2.1 State of the Art in Microgrids

The concept of microgrids goes back to 1882 with Thomas Edison when he constructed his first power plant (the Manhattan Pearl Street Station). This is considered a microgrid since the centralized utility grid had not been established yet. His company installed 58 DC microgrids by 1886 [9].

2.1.1 Microgrid components

The microgrid is assumed to be radial with several feeders and loads as shown in figure 2.1. It is connected to the utility grid distribution system through a point of common coupling (PCC), which is usually a static switch separation device. The microgrid includes a low-voltage network, loads, distributed energy resources (DER), switches and a hierarchical controller used to monitor and control loads and sources. The head of this controller is called the microgrid central controller (MGCC). The MGCC sends set point messages to the loads and local controllers at each source level, to control active power, reactive power, voltage levels and frequency. Also it sends messages to any switches in the microgrid to determine power flow paths.

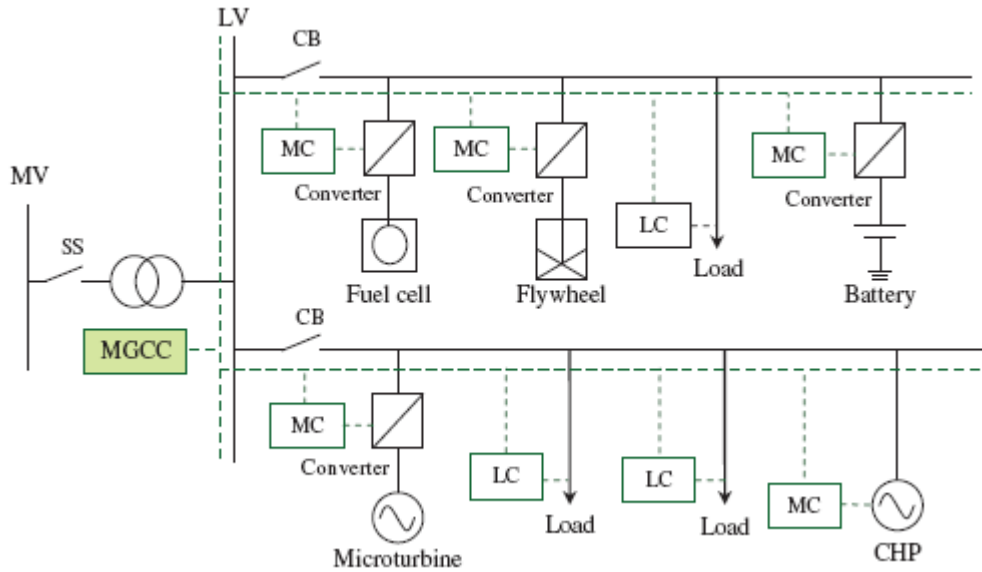


Figure 2.1: Basic Microgrid architecture with an MGCC [1]

DERs are small scale energy resources which can provide electricity locally to a load. A comprehensive review of common DERs in microgrids and their interactions is found in [10] and [11]. DERs include many technologies and are classified in two main categories: distributed generators (DGs) or energy storage systems (ESSs). DGs can be renewable such as wind, solar and geothermal sources. The use of renewable DGs in microgrids was extensively studied in literature. For example, [12] proposes a PV integrated building was proposed to run isolated from the utility grid in urban areas. Another example, [13], discussed the challenges that face the operation of wind turbines in capacity limited microgrids. The fluctuating nature of DGs necessitates the presence of an energy source for compensation. So energy storage systems enhance a microgrid's reliability, availability, and flexibility in energy generation, distribution and consumption.

2.1.2 Microgrid Operation

There are two modes of operation of a microgrid system: grid-connected mode and islanded mode.

- **Grid-Connected mode:**

In this mode, the microgrid is required to follow the utility grid distribution rules without participating in the operation of the main power system. The microgrid operates at the voltage and frequency set by the main grid. In this case, it acts as a controllable load or source. It can draw or supply power to the main grid. DERs are controlled through a hierarchical

three-level controller which will be discussed later. In [14], a method for optimal configuration of grid-connected microgrids based on probabilistic models is proposed. Probabilistic methods were used to describe wind and PV power on the microgrid. Energy management optimization was done for several grid-connected microgrids in [15]. The microgrids can exchange power locally between each other and with the main utility grid.

- **Islanded mode:**

Islanded operation or what is known as grid-forming mode or stand-alone mode when the microgrid is disconnected from the main utility grid. It can be islanded intentionally (all time or scheduled) or due to a failure. All microgrid components such as DERs, energy storage systems and loads operate independently as an isolated system. In this case and in the absence of the main grid, the distributed generator with the highest power rating is selected as a reference. All other distributed generators are controlled to follow its voltage and phase values. Islanded microgrids are mainly used in rural areas where there is no reach of a utility grid. Also it is used in remote military locations. Switching from grid-connected mode to islanded mode must be performed smoothly. In [16], a smart integrated adaptive centralized controller is proposed to monitor and control the operation of a microgrid in both intentional and unintentional islanding.

2.1.3 Microgrid Control

The operation of a microgrid requires energy management and classification of control strategies. The adjustment of voltage and frequency, synchronisation with the main grid and power flow control, all comprise the key principles of microgrid control structure [17, 18]. The control design should cover all the responsibilities of a microgrid's controller such as optimal power flow, maintaining stability, guaranteeing seamless connect/disconnect from the main grid, operating from black start, etc. [19]. [20] investigates several control strategies and energy management approaches of a microgrid.

According to the above-mentioned requirements, microgrid hierarchical controls are defined on four levels (from zero to three) shown in figure 2.2. Starting with the zero level (inner control loop) that controls voltage and current out of DERs and takes its reference values from level-one control (primary control). Then the level-two control (secondary control) monitors and supervises the system. Finally the level-three control (tertiary highest level control) manages power flow in the microgrid and between the microgrid and the main grid.

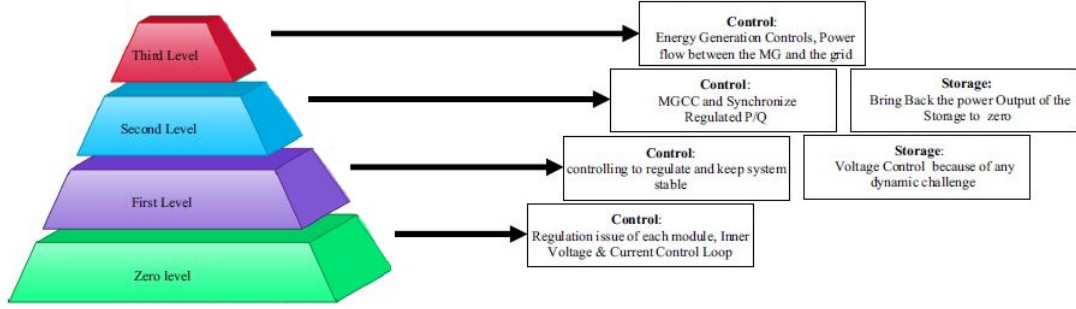


Figure 2.2: Hierarchical control of a microgrid [2]

2.1.3.1 Internal control loop

The aim of this level-zero control is to manage the power of DERs. It controls the source operating point using power electronic devices in current or voltage modes [17]. In the voltage control mode, a power electronic converter manages the voltage and frequency inside the microgrid (island mode) whereas in current control mode, it manages the active and reactive power (grid connected mode). The inner controls must have accurate reference values for frequency and voltage. These reference values are set by the primary controller.

2.1.3.2 Primary control

The aim of this level-one control is to adjust the voltage and frequency references to be fed into the inner voltage and current control loops. This control should have the fastest response to increase the system stability [21].

The P/Q droop control is an example of a control mode that provides set points to DER inverters [22], where the idea is for the inverter to mimic the droop characteristic of a synchronous generator. All DERs are connected via inverters where the active and reactive output at each inverter are as follows:

$$P_n = \frac{UU_n}{X_n} \sin(\delta_n) \quad (2.1)$$

$$Q_n = \frac{UU_n - U^2}{X_n} \quad (2.2)$$

where U is the integration voltage, U_n the output voltage of the inverter power supply, X_n the output impedance of the inverter power supply and δ_n is the angle between U_n and U .

It can be noticed from the above equations that the active power depends on δ_n (related to frequency) and the reactive power depends on the output voltage. So, the output voltage of the inverter is regulated by reactive power and the its frequency is regulated by active power. Figure 2.3 shows the P and Q droop control characteristics.

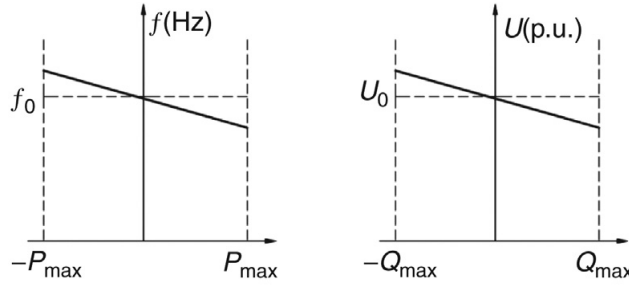


Figure 2.3: Voltage and frequency versus active and reactive power

2.1.3.3 Secondary control

The aim of this level-two control is to compensate for voltage and frequency deviations and regulate them towards zero at each change in load or generation. It corrects the deviations within an allowable limit $\pm 0.1 Hz$. The secondary control can be centralized or decentralized. In [23], a multi-microgrid cluster can be controlled by a hierarchical centralized controller.

2.1.3.4 Tertiary control

This control is used when the microgrid is in grid-connected mode. The purpose of this level-three control is to manage the power flow by regulating voltage and frequency. It measures P and Q at the point of common coupling (PCC) and compares them to the desired reference values. This level is the slowest level and ensures the optimal technical and economical operation of the microgrid. This controller is disabled in the case of islanding.

2.2 Fault-Tolerant and Multi-Parallel Power Converters

2.2.1 Fault Tolerance Levels of Power Converters

Power electronic inverters in a microgrid are very essential because they form the interface between DERs and the rest of the microgrid. Any fault that occurs in any inverter will result in the interruption of its operation and thus affecting the operation of the whole microgrid. The inverter and the whole microgrid are required to continue in operation even when a fault occurs. Fault tolerant inverters enhance the reliability of a microgrid system.

Fault diagnosis is the first step in a fault-tolerant system once a fault occurs [24]. Fault diagnosis uses complex algorithms to detect and specify the position and type of the fault in an inverter or a microgrid. In [25], a survey is performed on fault diagnostics in a smart microgrids. It first presents different failure modes

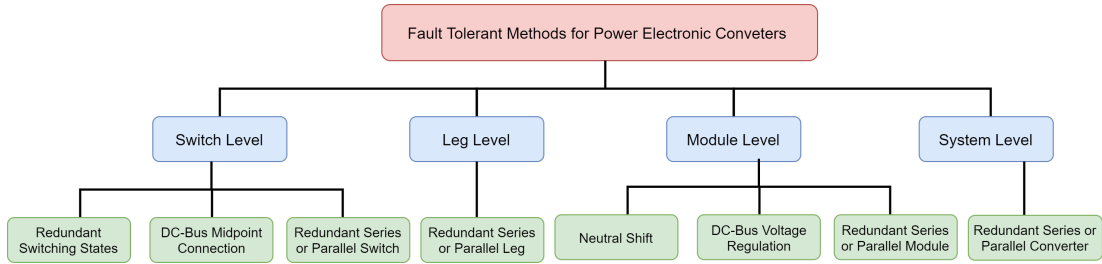


Figure 2.4: Fault tolerant methodology chart

in microgrids and categorises them into model-based and data-driven methods. In [26], the diagnosis is inside the inverter itself, where a generalised logic-based method for fault diagnosis in a multilevel inverter is presented. Many examples are available in the literature, and the thesis will elaborate on different types and examples.

The next step in a fault-tolerant system is to isolate the fault and reconfigure the power converter. Reconfiguration of a converter is usually based on hardware redundancy and it is classified to four categories according to the redundancy level: switch-level, leg-level, module-level and system-level [27]. See figures 2.4 and 2.5.

- **Switch-Level Reconfiguration**

Multilevel inverters can be considered one type of inherently switch-redundant circuits due to the abundance of switches when compared two-level inverter. Switch-level reconfiguration can be achieved in most power converters by installing redundant switches in series or parallel [28]. Redundant switches added in parallel don't operate in normal conditions. When a fault occurs, the redundant switch can replace the faulty switch via a selecting relay. The series redundant devices are connected in series with main switches for short-circuit failures.

- **Leg-Level Reconfiguration**

This approach is implemented via adding a parallel redundant leg in an inverter. The number of added legs can be from 1 to 3 [29]. The backup leg can operate in online or offline mode. Linking switches are required in the offline scheme. The loss is higher in the online mode due to the fact that the additional leg is operating.

- **Module-Level Reconfiguration**

Module-level solutions are primarily in cascaded multilevel converters which are typical circuits which use module redundancy. When a module fails, the other modules implement the fault-tolerant reconfiguration to

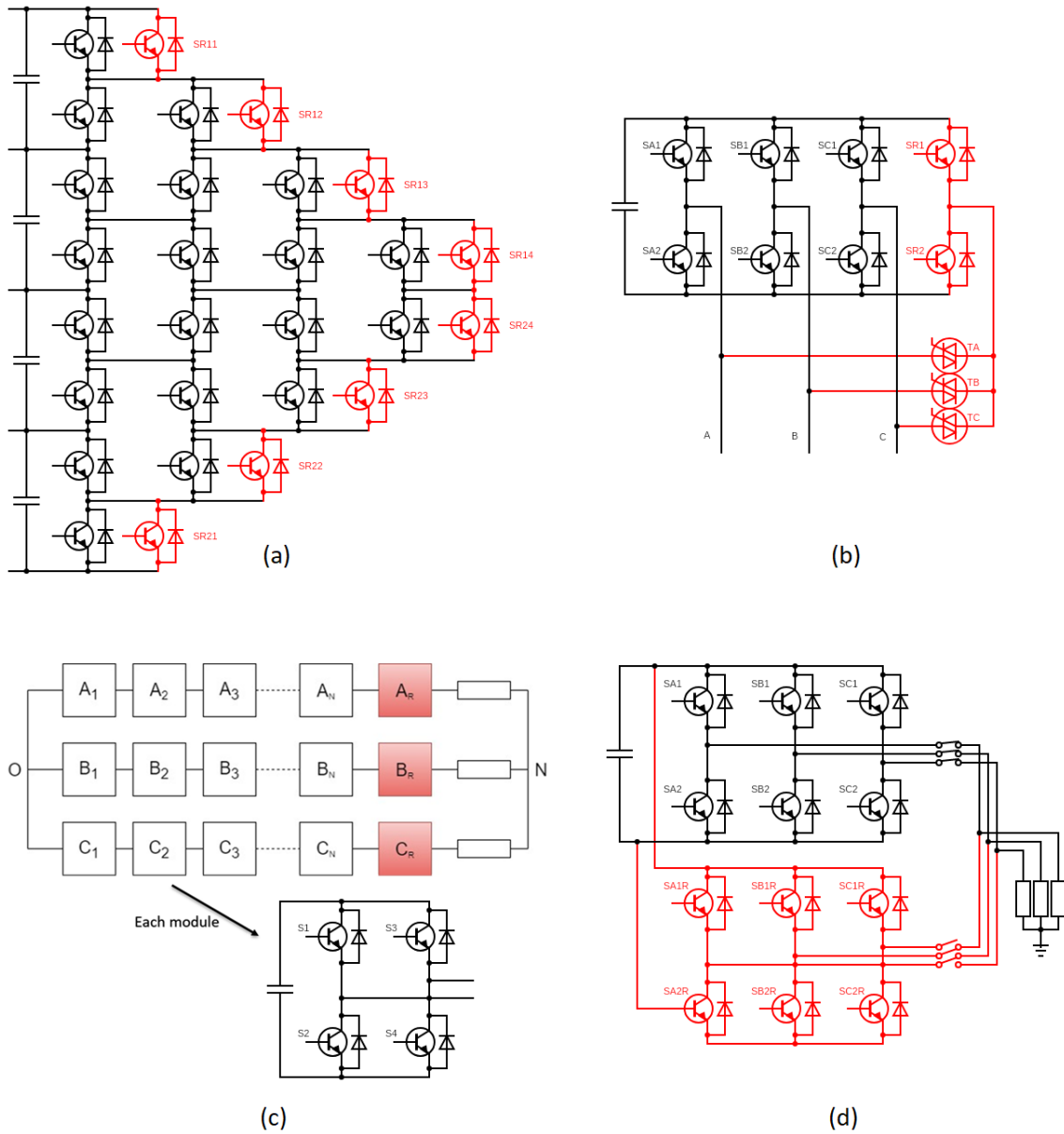


Figure 2.5: Fault tolerant inverters topologies. (a) Switch level. (b) Leg level. (c) Module level. (d) System level.

maintain continuous operation. The main approaches are neutral shift, dc bus regulation, and redundant module installation.

When a fault occurs in a certain module, an unequal number of modules appears at each phase and thus a phase shift from the reference occurs. Thus, the neutral is shifted to retain the voltage balance [30]. The DC bus reconfiguration is achieved by increasing the dc link of other working modules during a fault. This is to keep the total output voltage RMS or peak value unchanged [31].

- **System-Level Reconfiguration**

System-level reconfiguration is the highest level of hardware reconfiguration. This method depends on adding complete redundant inverters in parallel or cascaded with nominal inverters. An example of system-level redundancy is using parallel inverters to improve the reliability of uninterruptible power supply (UPS) systems [32].

2.2.2 Parallel Multi-inverters in a Microgrid

It is important to note that our proposed solution for fault tolerance depends on using the existing inverters without adding external redundancy, and operating inverters themselves as backup inverters in fault scenarios. This will be explained in section 3 in detail. Meanwhile, it is essential to mention that the proposed method is considered a system-level fault tolerance solution, in which there are multiple inverters operating in parallel. Many studies are found in the literature that aim to control parallel power converters. In [33], the circulating current between two parallel three-phase rectifiers is controlled. The paper develops a zero-sequence model to predict the dynamics of zero-sequence current. It then introduces a new control variable and a strong control loop to suppress the circulating current. [34] proposes a network communication system applied in a control strategy for parallel multi-inverters; a master-slave mode is employed with two analog and digital busses, where the master sends reference messages to the slaves. An optimal control was used to control current sharing between multi-inverter system in [35]. A state-space model was derived for the system with the inverters' currents as states. This method can be used to mimic the scenario if a fault on an inverter by simply setting a zero-reference value for a certain inverter current state. In [36], also a state space model was derived for a multi-paralleled grid-connected inverters but with LCL filters. The benefit of these filters is to prevent the main grid from being polluted with harmonics. A shunt active power filter based on parallel interleaved inverters was studied in [37]. The paper gives a practical and low cost solution for minimizing circulating current by installing common-mode inductor on each inverter.

Chapter 3

Proposed Solution for Retrieving Lost Power

As shown in the previous literature, most fault-tolerant techniques depend on adding hardware redundancy at different levels of an inverter, or utilizing switch-level redundancy in multi-level topologies. Also, a diagnosis analysis must be run to specify the fault location to deal with and engage appropriate redundancy or reconfiguration. Diagnosis algorithms are usually complex and require accurate sensing and fast processing.

The proposed method in this thesis tries to find a topology that does not require any additional hardware redundancy, but depends on the available inverters in the microgrid. Also there is no need to run fault diagnosis algorithms, only basic fault detection algorithms.

3.1 Bidirectional switch

When a fault occurs in any inverter in the microgrid, the power generated by the corresponding source will be lost and will not be transmitted to the main grid. The idea is to benefit from this curtailed power by rerouting it to another available inverter. A bidirectional switch will be added to the microgrid topology. It connects the two branches of the inverters as shown in figure 3.1. During normal operation, the switch is always open. It functions only when a fault is detected in an inverter, where it closes to form a route for the curtailed power through another healthy inverter. This switch should thus be a controlled bidirectional switch. Figure 3.2 shows several topologies of such switch realizations.

3.2 Fault Scenario

The output voltages of the inverters are always sensed and monitored. Once a deviation from the normal values is detected in an inverter, it will be considered

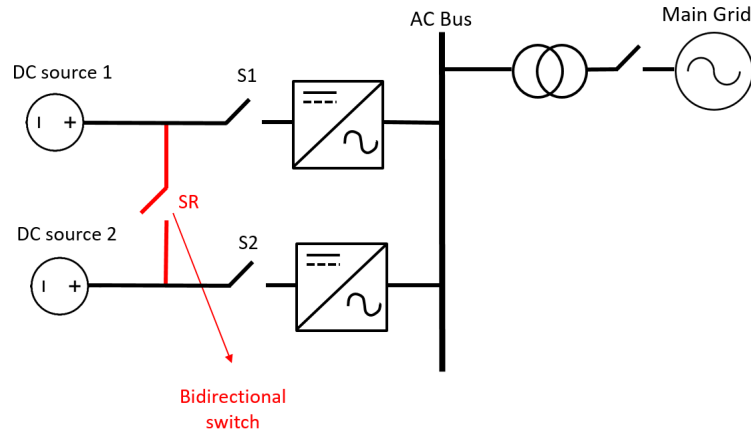


Figure 3.1: Bidirectional switch addition

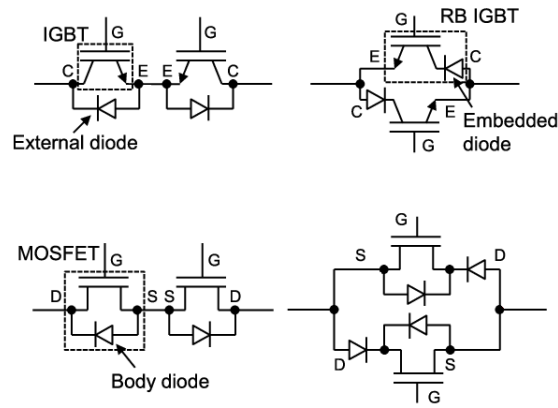


Figure 3.2: Bidirectional switch realizations

faulty. This is a very basic fault detection algorithm, which does not require any significant data processing or complex algorithm. Thus, there is no need to run a diagnosis algorithm to know where is the fault inside the inverter since the faulty inverter will simply be isolated from the microgrid. The other existing and healthy inverter will work as a backup when not working at its maximum rating. In that case, the power of the faulty inverter is rerouted to the healthy one via the controlled bidirectional switch.

The available power at each inverter is fed to the controller of the bidirectional switch to switch ON/OFF accordingly. It will be calculated from the solar irradiance which can be collected from an available sensor or from a predictive model.

For example, suppose in figure 3.1 the inverters are connected to solar panels and rated at 1000 W each. Assume that the available solar power from the solar PV panels is 300 W. If a fault occurs at the top inverter, the second inverter can handle the additional 300 W lost from the first inverter. If the second inverter

is operating at its maximum capacity or can't handle the combined power, the switch remains open and it does not interfere with the microgrid. Also, the voltages of the DC sources must be approximately equal before closing the switch. This is to minimize the shoot-through current on switching. Figures 3.3 and 3.4 show the energy routing and the switching algorithm flowchart respectively.

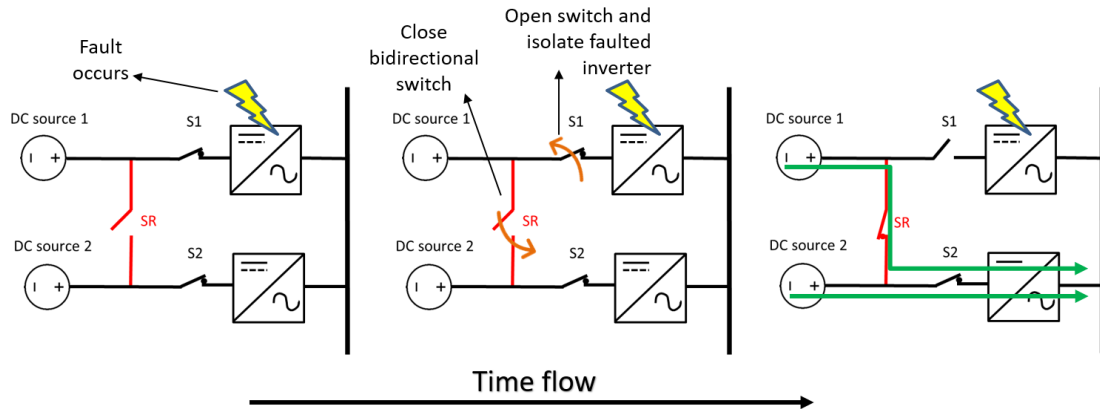


Figure 3.3: Fault scenario

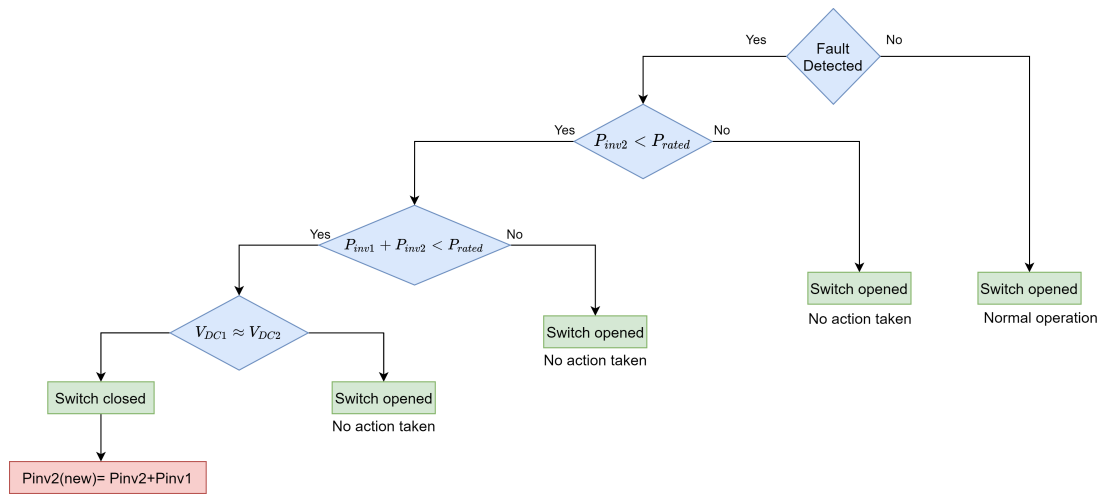


Figure 3.4: Switching algorithm flow chart

Chapter 4

Microgrid and Algorithm simulation

4.1 Application in PV Systems

In this section, two solar arrays of 50 KW power each are connected to the main grid via two three-phase inverters each rated at 60 KW each. The inverters are controlled such that the solar panels work in the Maximum Power Point Tracking (MPPT) mode. This is to harness the maximum available solar energy and inject it on the main grid. The controlled bidirectional switch explained in chapter 3 is added between the panels. Figures 4.1 and 4.2 show the schematics of grid-connected solar panels and inverters' control blocks respectively. The PV arrays are fed with solar irradiance of half-sine that maximizes at $1000 W/m^2$. Note that the time of the irradiance profile is reduced to accelerate the simulation.

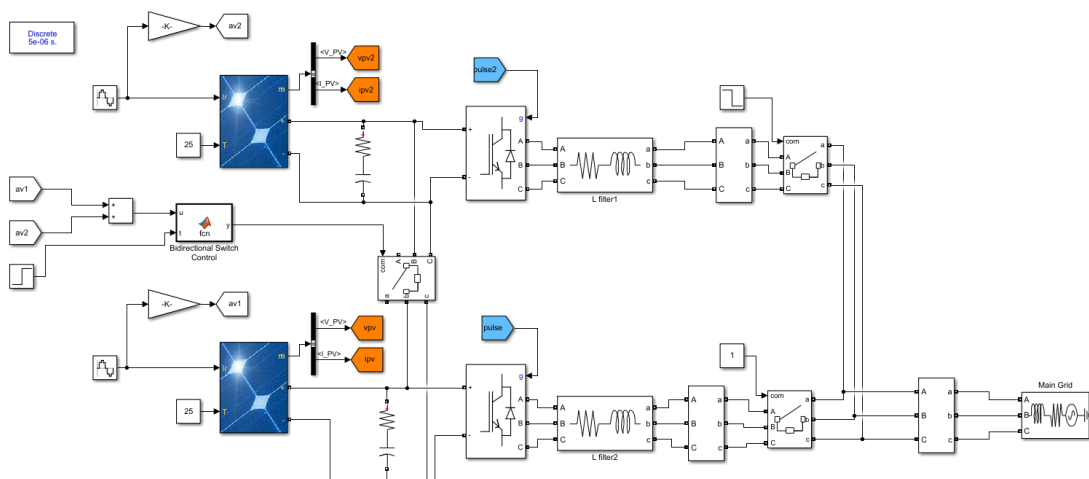


Figure 4.1: MATLAB Simulink schematic of grid connected solar arrays

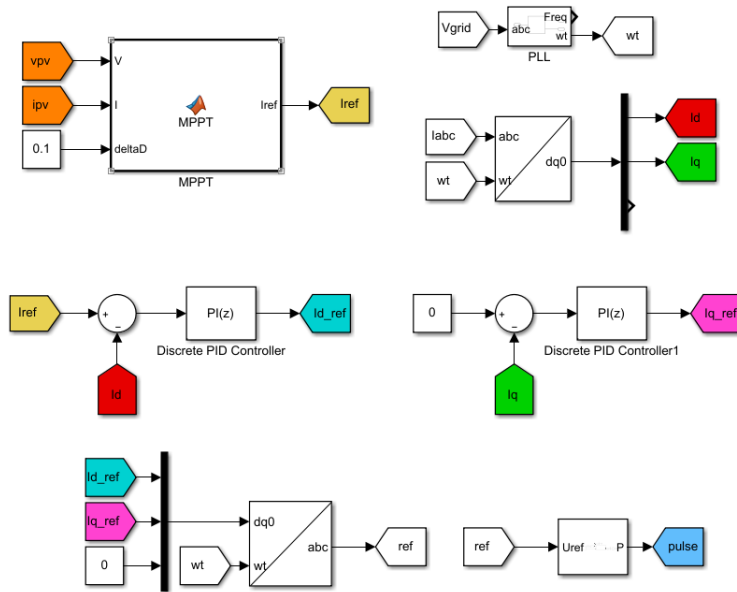


Figure 4.2: Control blocks of the inverters

4.1.1 Normal Operation

During Normal operation, the two solar arrays are disconnected from each other. Their corresponding inverters are working independently applying the MPPT algorithm. Power generated is injected to the main grid at the PCC. Only real power is injected into the grid, even though the utilized controller can inject reactive power as well. Figures 4.3 - 4.9 show the system performance during normal operation. Each inverter is maximizing at 50 KW (Figure 4.7) and summed up to inject 100 KW to the main grid as shown in figure 4.6.

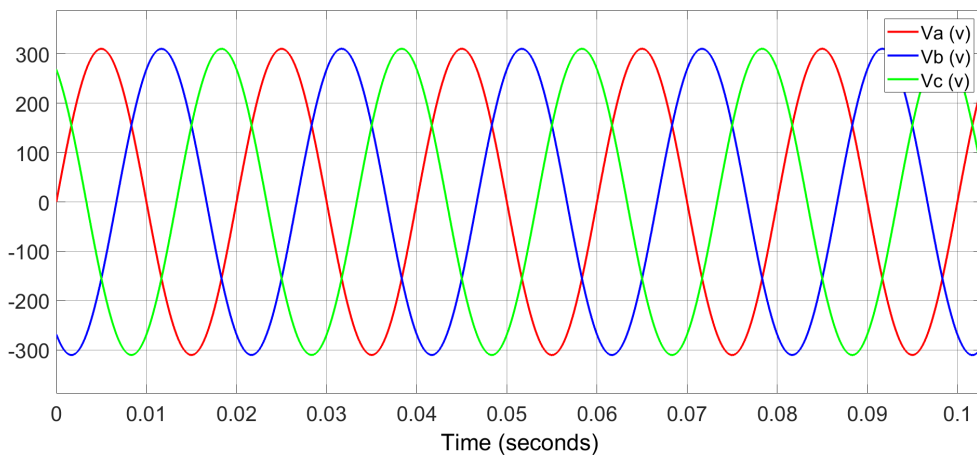


Figure 4.3: Three phase grid voltage

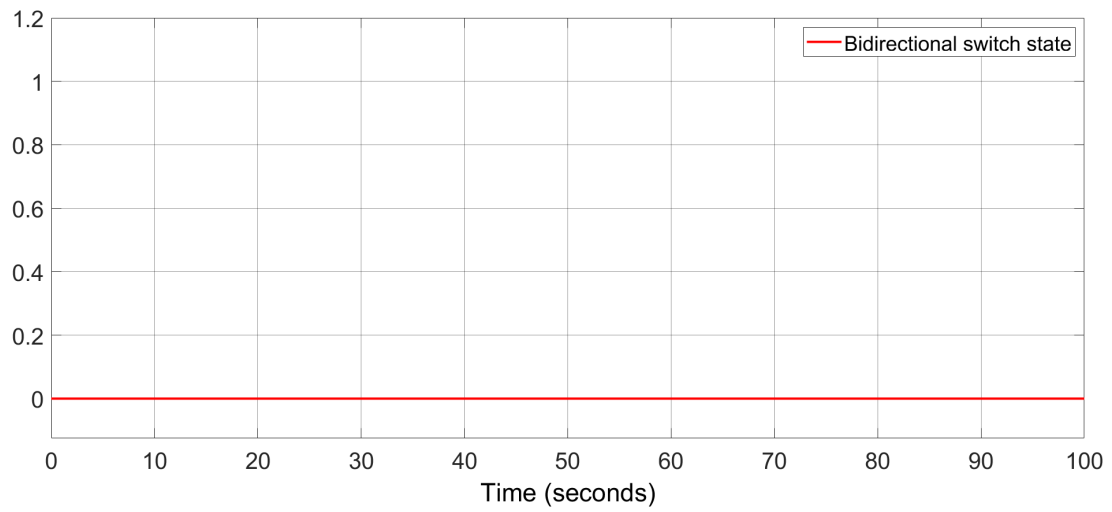


Figure 4.4: Bidirectional switch state in normal operation

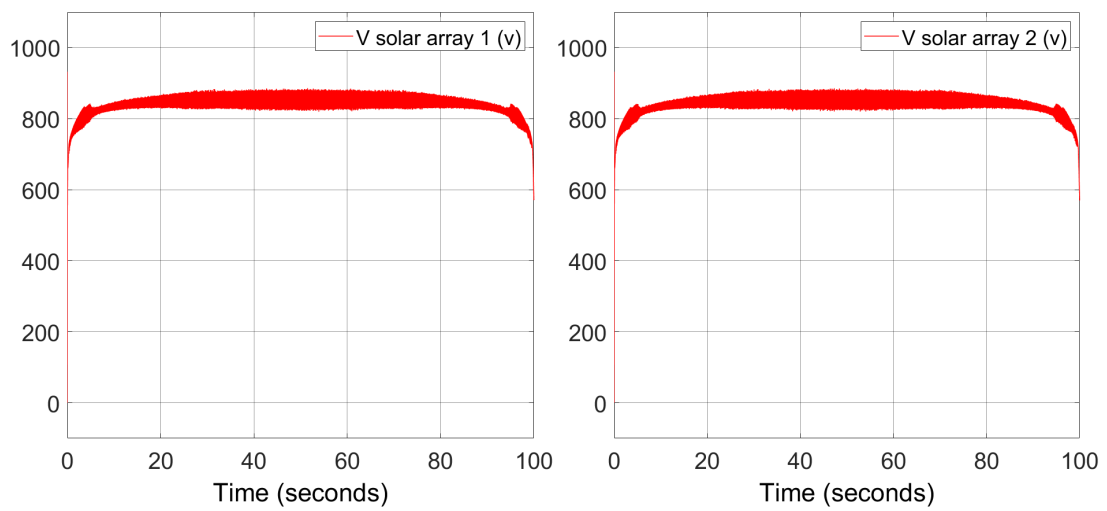


Figure 4.5: Solar arrays DC voltage in normal operation

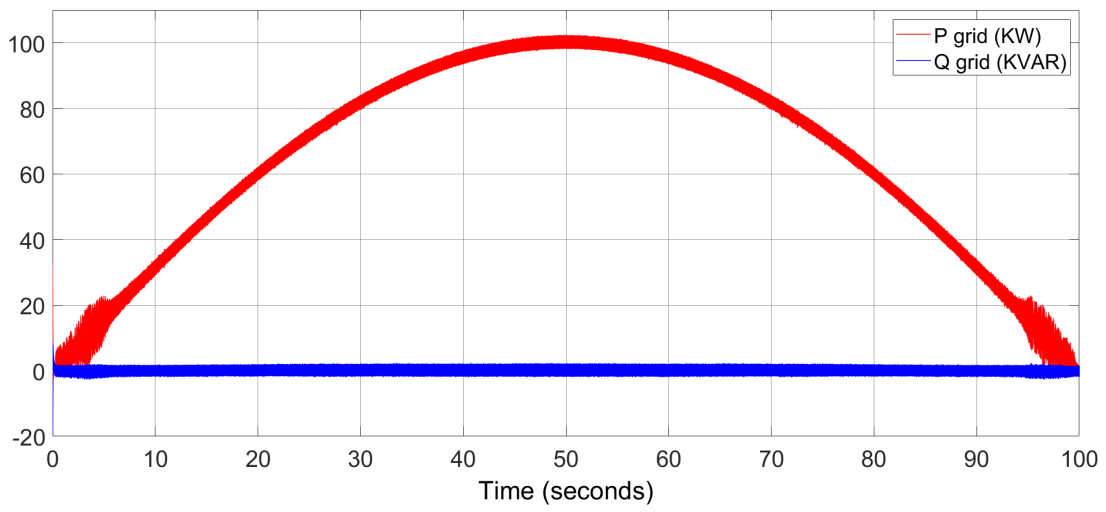


Figure 4.6: Power injected to grid in normal operation

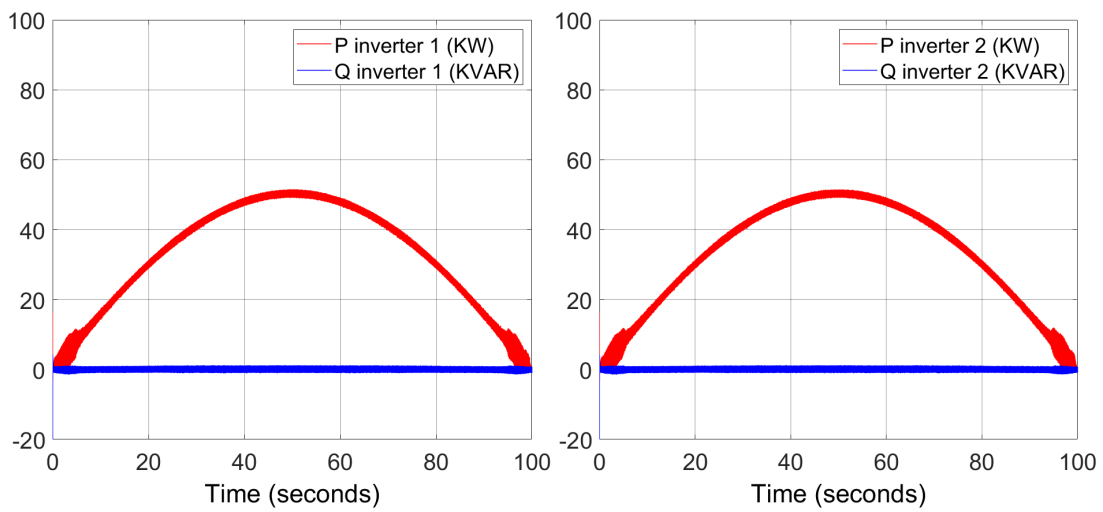


Figure 4.7: Power output of inverters in normal operation

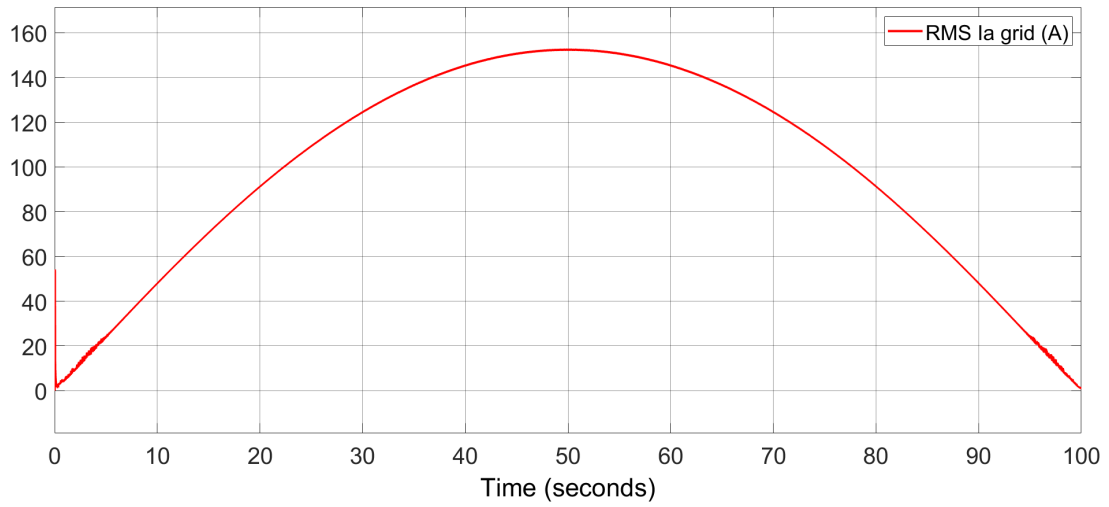


Figure 4.8: Phase 'a' RMS current injected to grid in normal operation

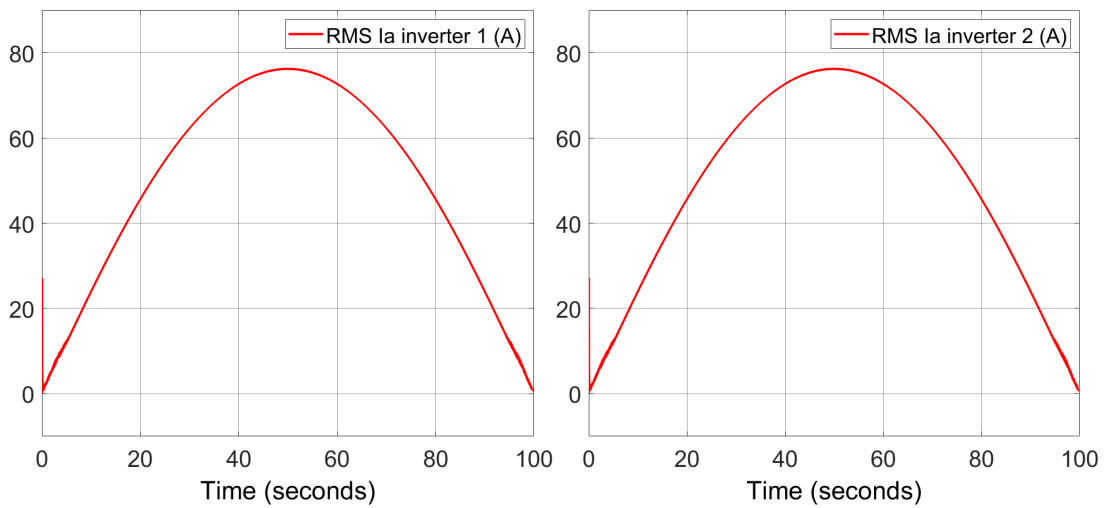


Figure 4.9: Phase 'a' RMS output currents of inverters in normal operation

4.1.2 Fault Operation

The bidirectional switch at first is opened. Once a fault is detected in an inverter, it is immediately isolated from the main grid. Then the bidirectional switch will be ready to close and operate after 2s of the fault. Although the switch will be ready to close but this won't happen unless the inverter can hold the total power. The available power is calculated. If its higher than the healthy inverter ratings, the switch will stay opened. Once the available power falls below the allowed rating, the switch will close and form a route that passes power from the isolated array to the healthy inverter. Two scenarios were simulated where the fault is emulated at two different instances.

4.1.2.1 Fault at $t=10s$

The fault is emulated at instance $t=10s$ on inverter 2. As shown in figure 4.12, the grid power is reduced to half as the faulty inverter is isolated immediately. The bidirectional switch closes at $t=12s$ connecting the corresponding solar array to the healthy inverter. Then it opens at $t=21s$ due to the fact that the available power from both arrays exceeds the rating of the healthy inverter (60KW). After that it closes again at $t=79s$ when the available power is below the healthy inverter ratings. Figures 4.10 - 4.15 illustrate the performance of the system during this fault scenario.

It is noted that at $10s < t < 12s$ and $21s < t < 79s$, the DC voltage of the PV array corresponding to the faulty inverter is higher (see figure 4.11). This is the open-circuit voltage (V_{oc}) of the PV arrays as they are isolated during these times.

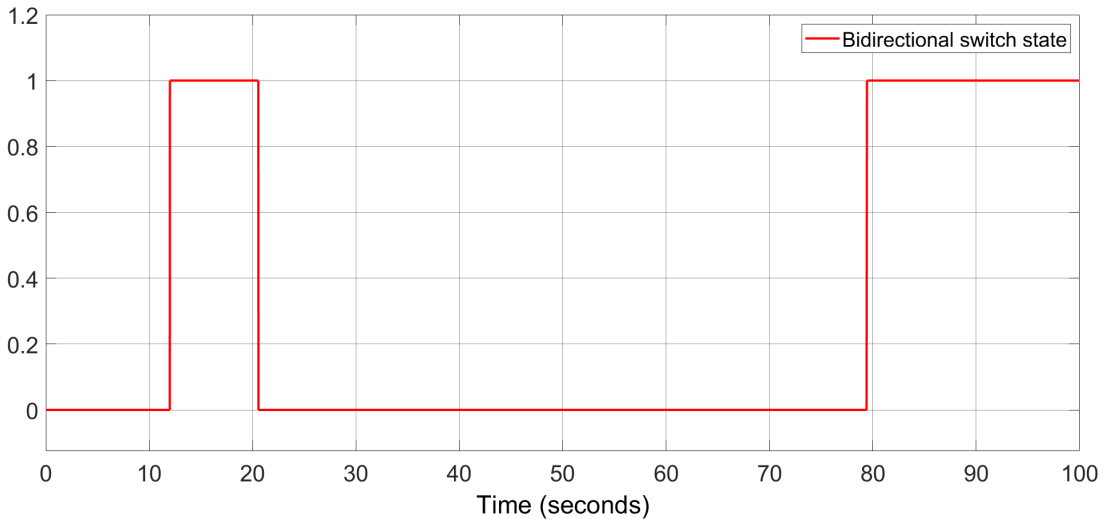


Figure 4.10: Bidirectional switch state (fault at 10s)

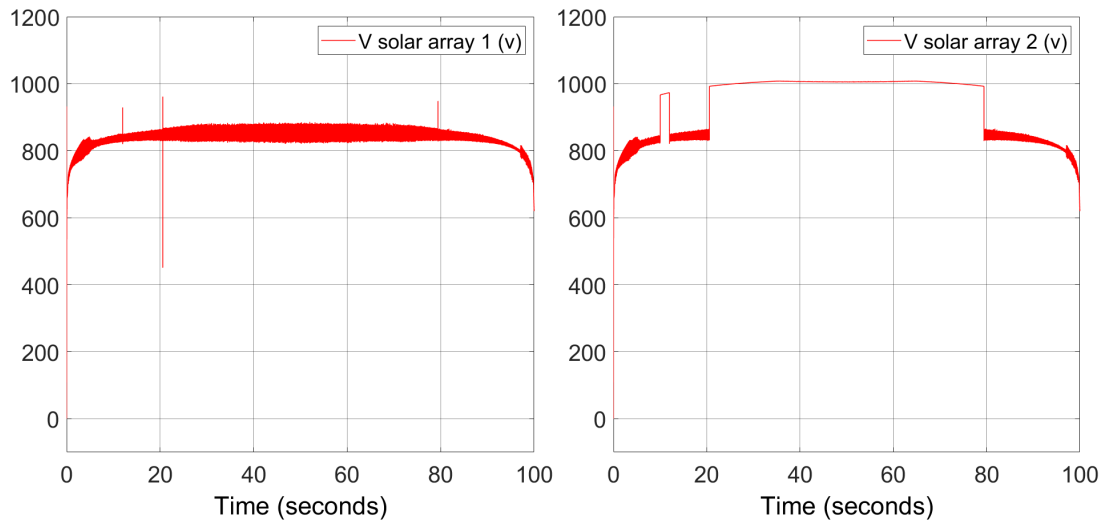


Figure 4.11: Solar arrays DC voltage (fault at 10s)

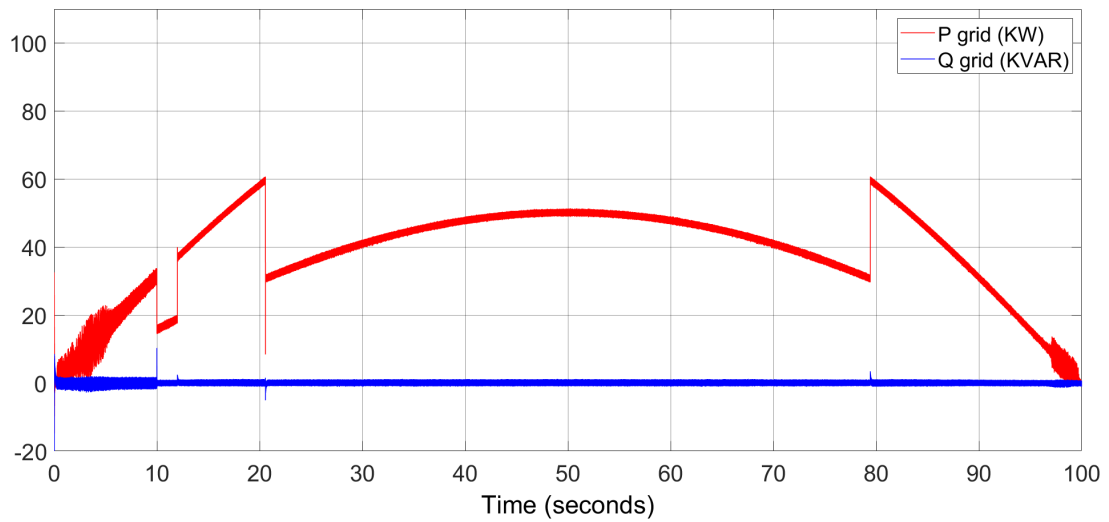


Figure 4.12: Power injected to grid (fault at 10s)

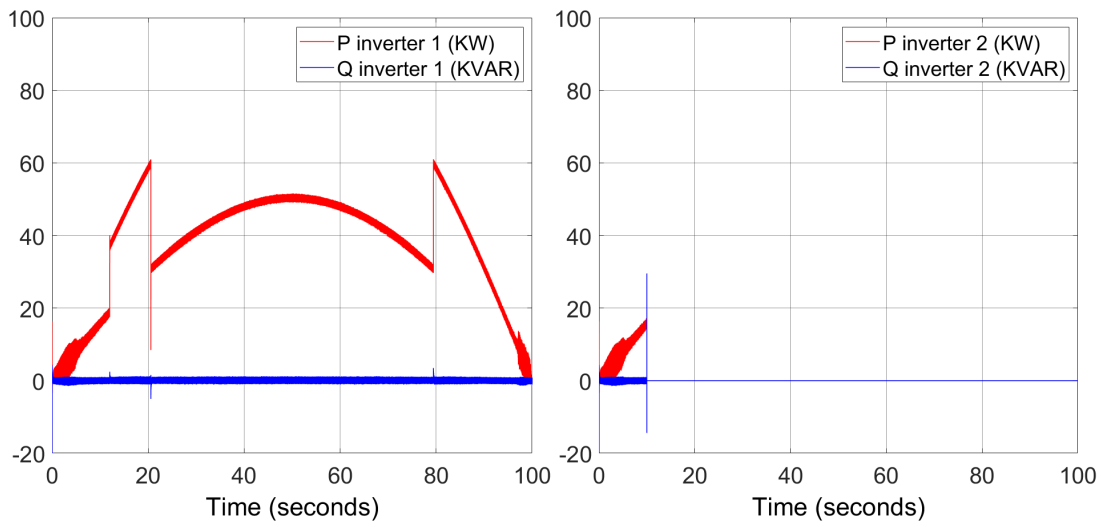


Figure 4.13: Power output of inverters 1 (healthy) and 2 (faulty) (fault at 10s)

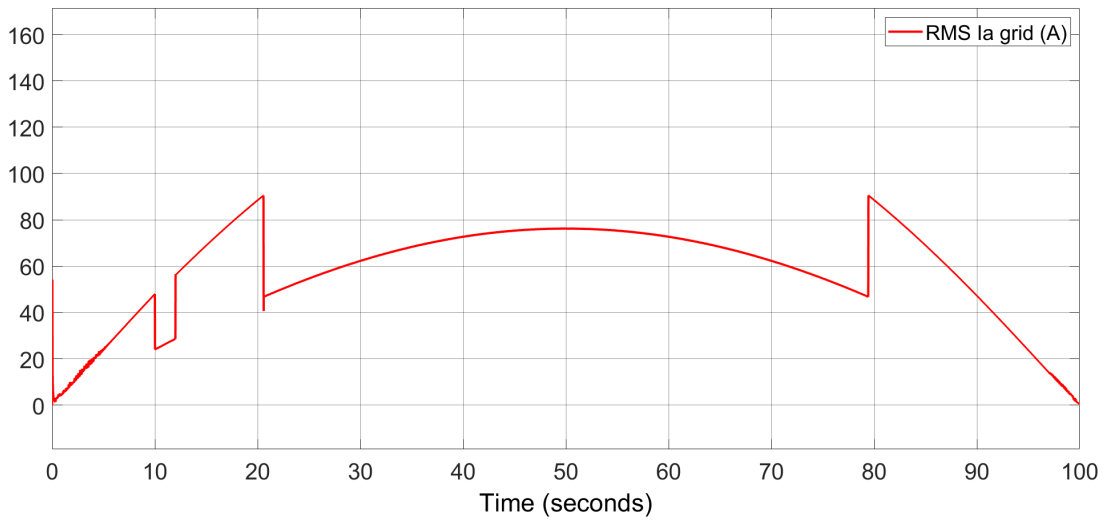


Figure 4.14: Phase 'a' RMS current injected to grid (fault at 10s)

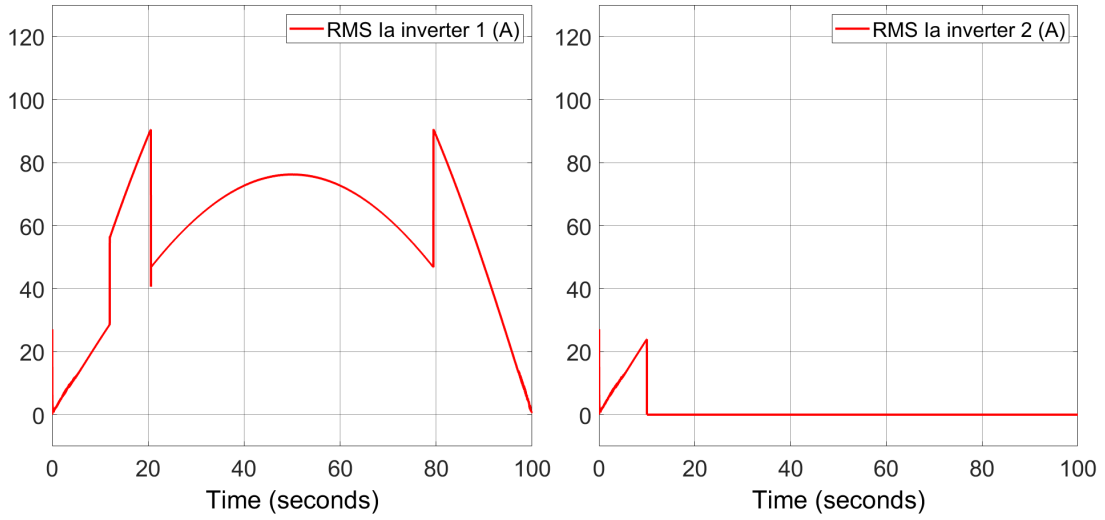


Figure 4.15: Phase 'a' RMS output currents of inverters 1 (healthy) and 2 (faulty) (fault at 10s)

4.1.2.2 Fault at $t=50s$

Here the fault is emulated at the peak time $t=50s$. The bidirectional was ready to close at $t=52s$ but it closed at $t=79s$ when the healthy inverter was capable to hold power from both solar arrays. Figures 4.16 - 4.21 illustrate the performance of the system during this fault scenario.

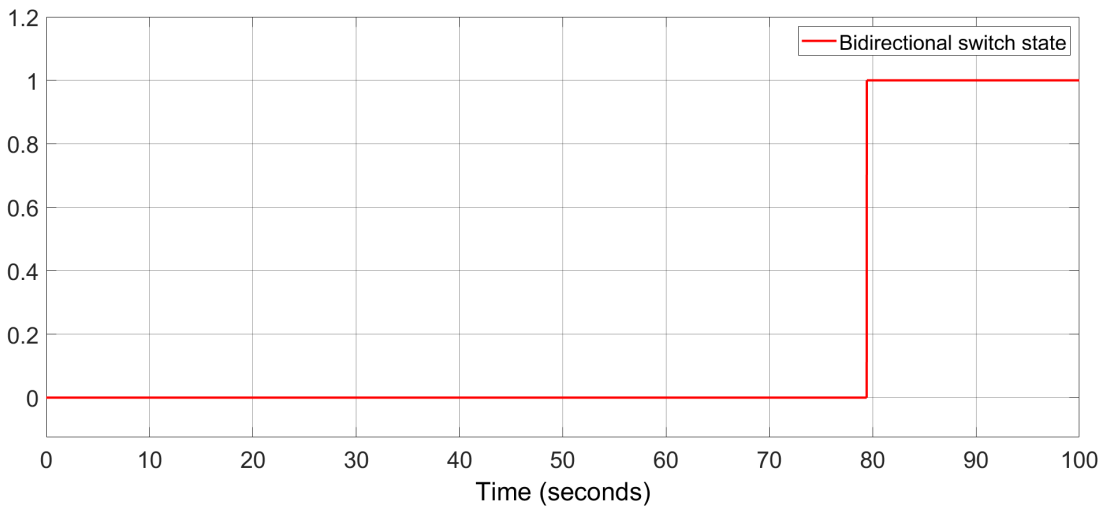


Figure 4.16: Bidirectional switch state (fault at 50s)

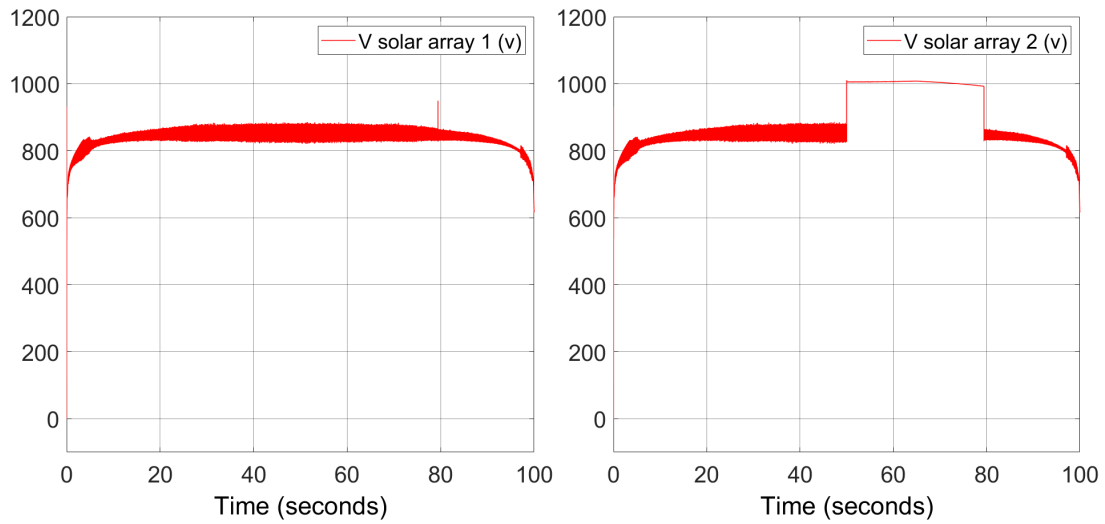


Figure 4.17: Solar arrays DC voltage (fault at 50s)

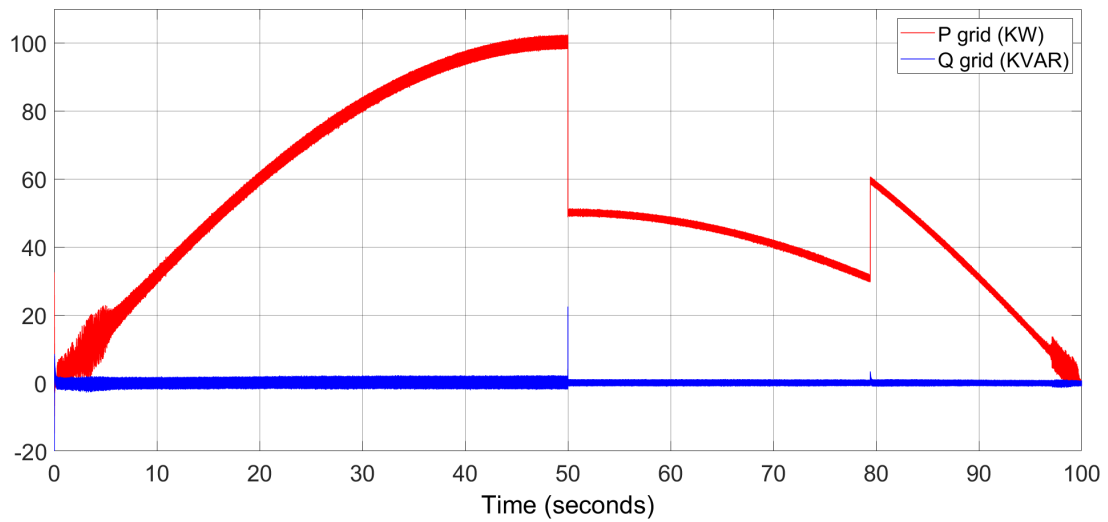


Figure 4.18: Power injected to grid (fault at 50s)

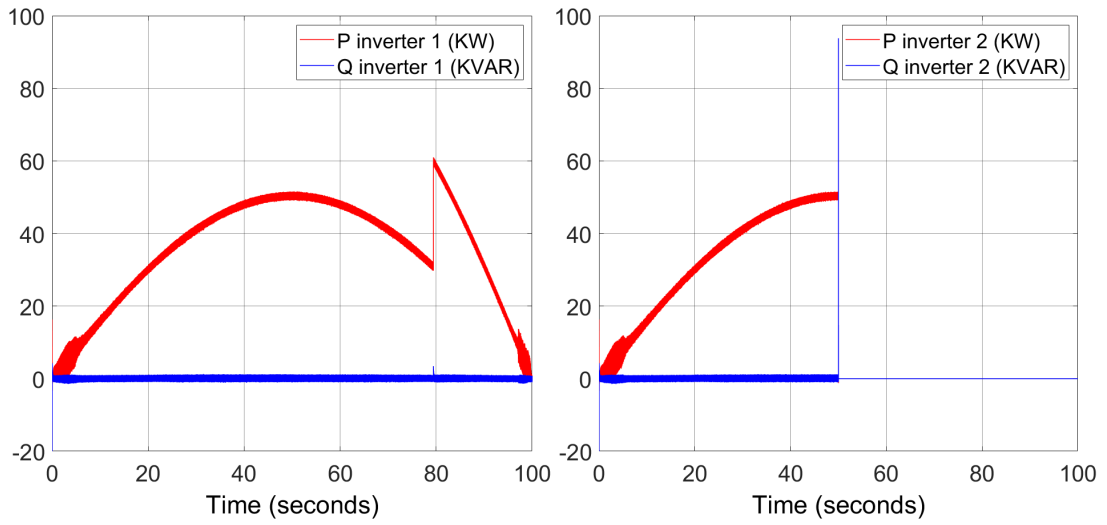


Figure 4.19: Power output of inverters 1 (healthy) and 2 (faulty) (fault at 50s)

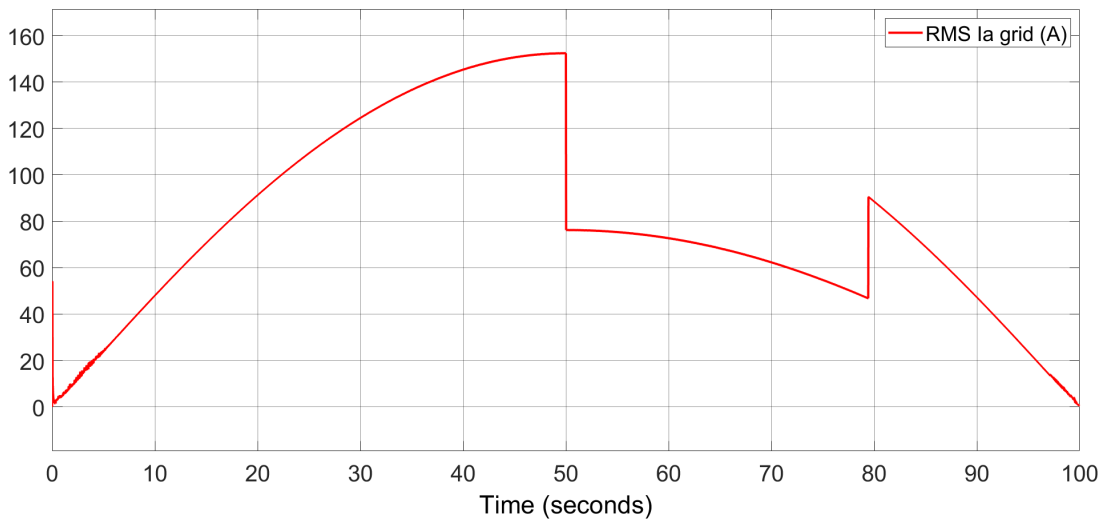


Figure 4.20: Phase 'a' RMS current injected to grid (fault at 50s)

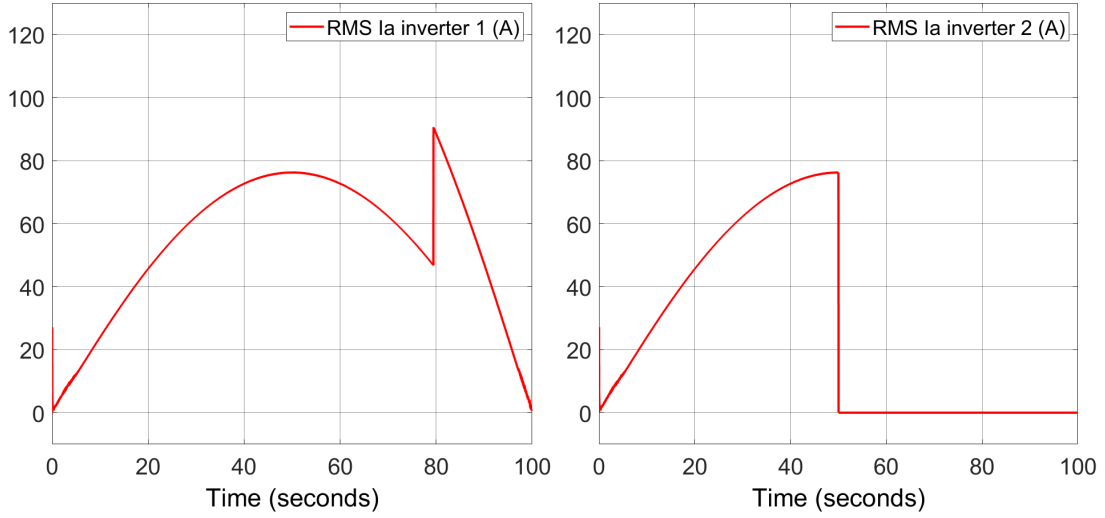


Figure 4.21: Phase 'a' RMS output currents of inverters 1 (healthy) and 2 (faulty) (fault at 50s)

4.1.3 Advantages

Advantages of applying this solution on solar panels are the following:

- Enhancing the reliability of the whole microgrid. The inverter now can operate more than one solar array rather than being locked to only one array. This can give more solution opportunities within a short time rather than waiting for the inverter maintenance
- There is no need to run a complex fault detection diagnosis. Simple sensing of inverters' output voltages can indicate for any fault and thus isolating the corresponding inverter and closing the bidirectional switch.
- Reducing the curtailed power when routing it to other inverter and thus increasing the harnessed energy. The saved power in the scenario 2 (fault at 10s) for example can be calculated as follow:

$$\begin{aligned}
 \text{Energy retrieved} &= \text{Energy with method} - \text{Energy without method} \\
 &= \int_{12}^{21} (100 \sin 0.01\pi t - 50 \sin 0.01\pi t) dt \\
 &+ \int_{79}^{100} (100 \sin 0.01\pi t - 50 \sin 0.01\pi t) dt \\
 &\approx 15 \text{ Wh}
 \end{aligned} \tag{4.1}$$

4.1.4 Operation Under Realistic Solar Irradiance

The previous simulations were done on 100s seconds scale for reducing simulation time and computations. In this section, a slot of time was taken from a typical day in Beirut with a realistic solar irradiance. On the first of June at 5:00 am, the available solar irradiance is 360 W/m^2 and increased to 580 W/m^2 at 6:00 am. The data for Lebanon is got from the "European Commission's science and knowledge service" [38].

The simulation was run for 10 minutes (600 seconds) from 5:00 am to 5:10 am where the irradiance reaches 400 W/m^2 as shown in figure 4.22. The fault was emulated on inverter 2 at $t= 300\text{s}$ (5:05 am) where the bidirectional switch closes after 20 seconds connecting both solar arrays to the healthy inverter 1. Figures 4.23 and 4.24 show the power injected to grid and output power of inverters.

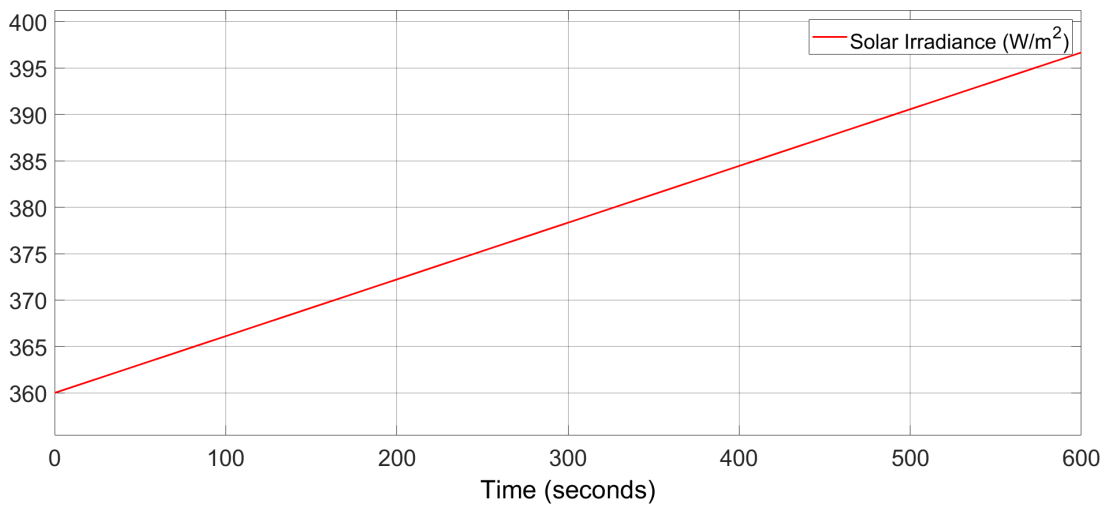


Figure 4.22: Solar irradiance in Beirut at 5:00 am till 5:10

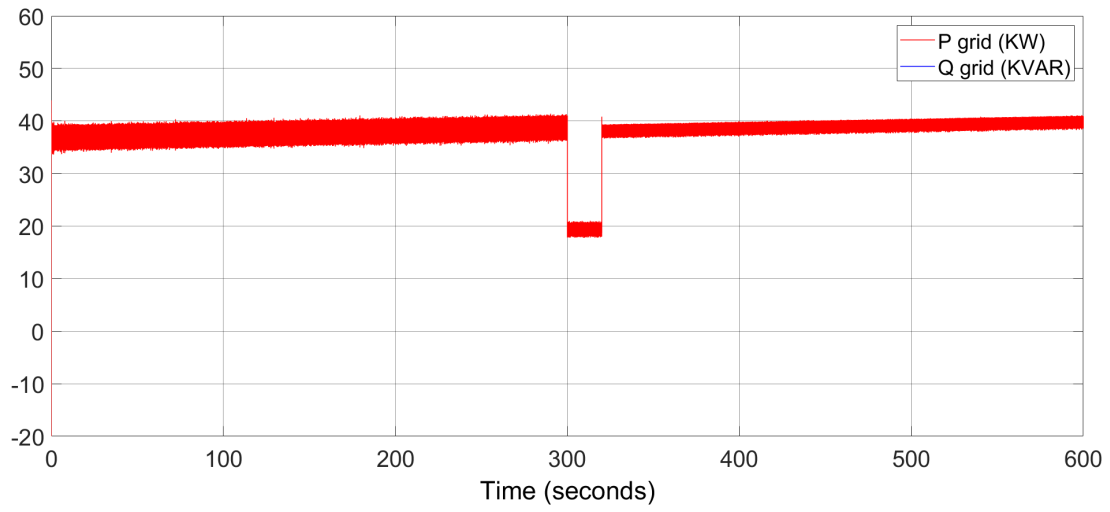


Figure 4.23: Power injected to grid under realistic solar irradiance

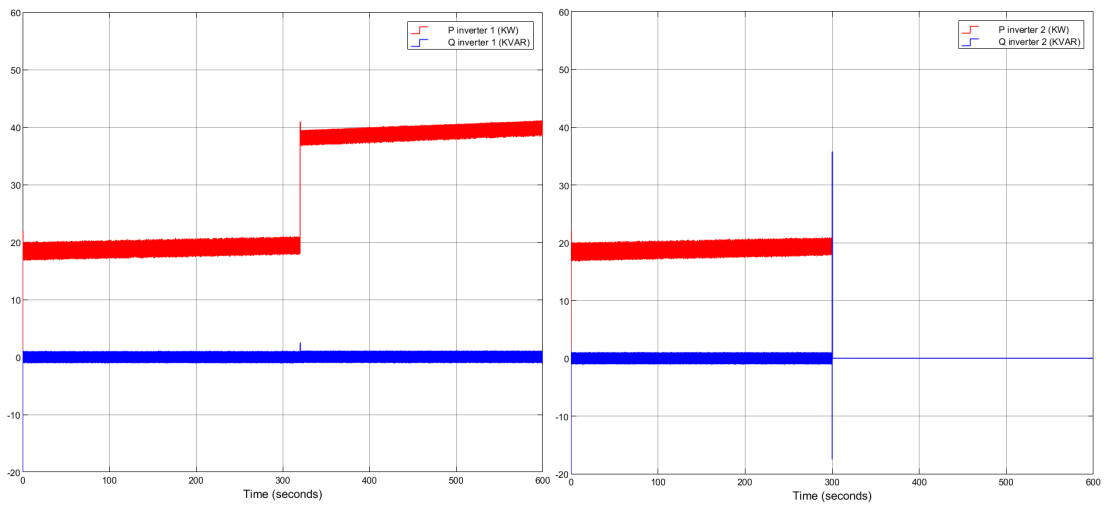


Figure 4.24: Power output for inverters under realistic solar irradiance

4.2 Application in Battery Systems

The proposed method is also applied to a battery ESS. Two battery banks are connected to the main grid via two three-phase inverters rated at 60 KW each. The inverters are controlled to work in power-demand mode. The controlled bidirectional switch is added between the banks. Figures 4.25 and 4.26 show the schematics of grid connected storage banks and inverters' control blocks respectively.

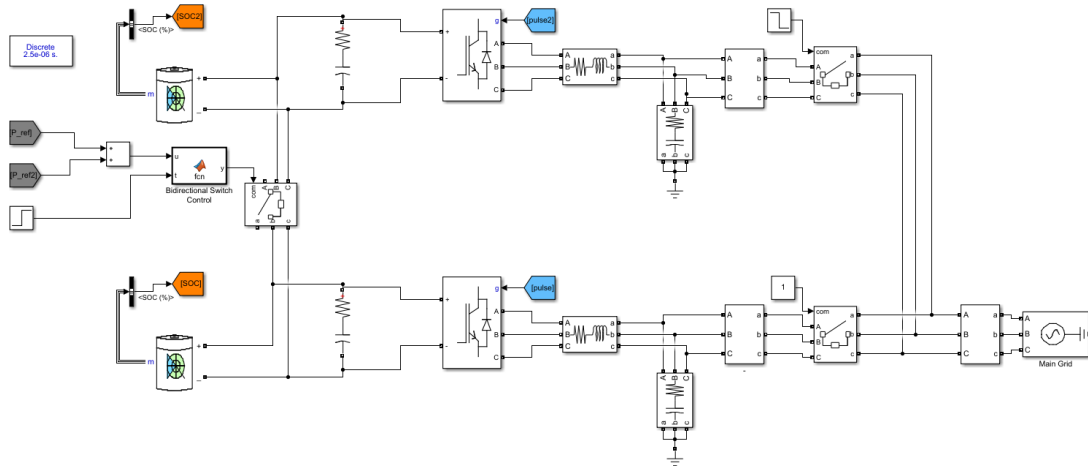


Figure 4.25: MATLAB Simulink schematic of grid connected storage banks

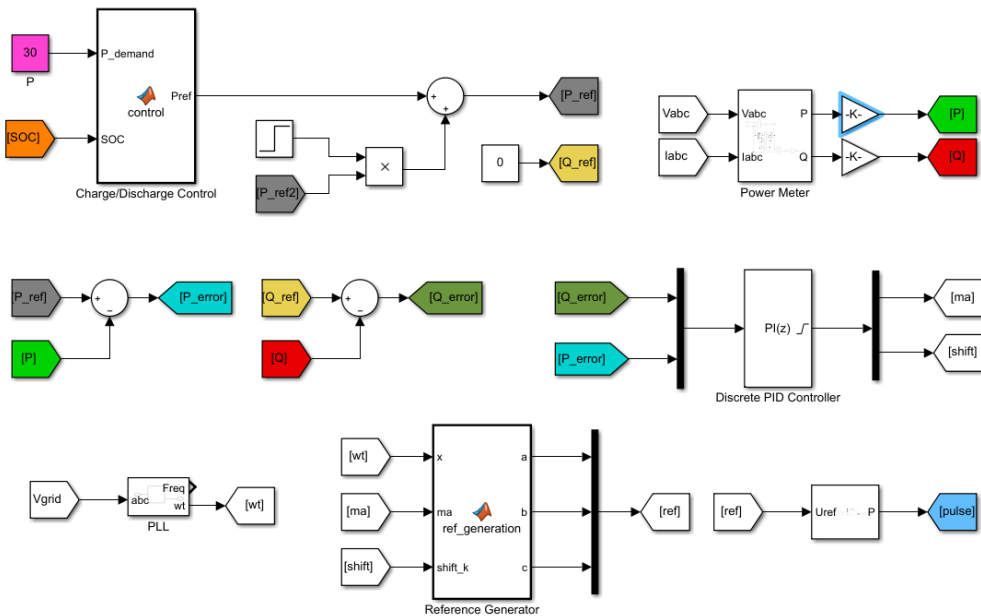


Figure 4.26: Control blocks of the inverters

4.2.1 Normal Operation

4.2.1.1 Active Power Generation

During Normal operation, the two solar arrays are disconnected from each other. Their corresponding inverters are working independently applying the power demand algorithms. It is set on 20 KW and 10 KW for first and second inverters, respectively. The power generated is injected to the main grid at the PCC. Only real power is injected into the grid, even though the utilized controller can inject reactive power as well. Figures 4.27 - 4.33 show the system performance during normal operation. Each inverter is supplying its reference set power (Figure 4.30) and summed up to inject 30 KW to the main grid as shown in figure 4.29.

The state of charge (SoC) of the batteries are controlled to stay within the [20%, 80%] interval during charging/discharging process. This is to protect the batteries from over charging/discharging and extend their life time. The initial SoC of both storage banks is 80% as shown in figure 4.31.

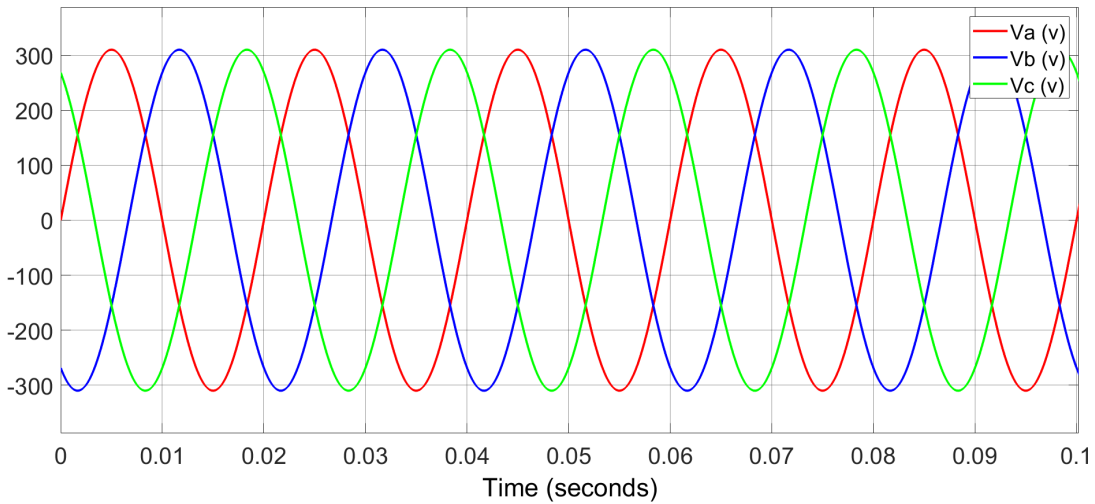


Figure 4.27: Three phase grid voltage

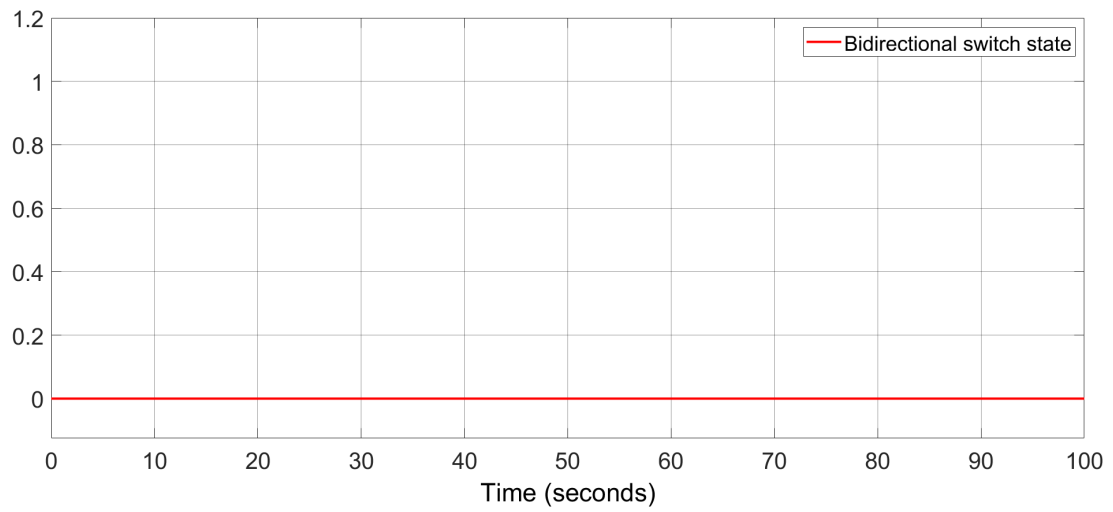


Figure 4.28: Bidirectional switch state in normal operation

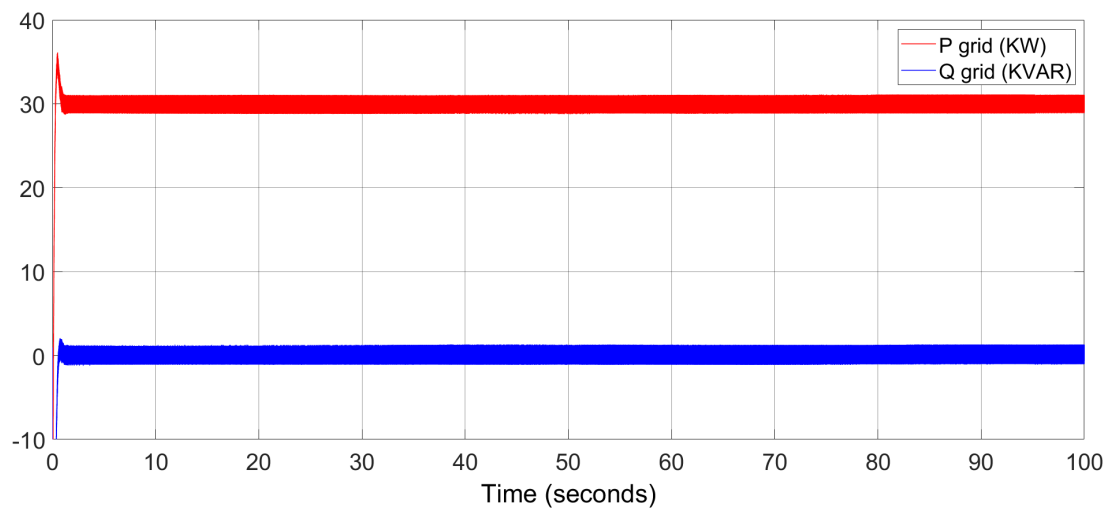


Figure 4.29: Power injected to grid in normal operation

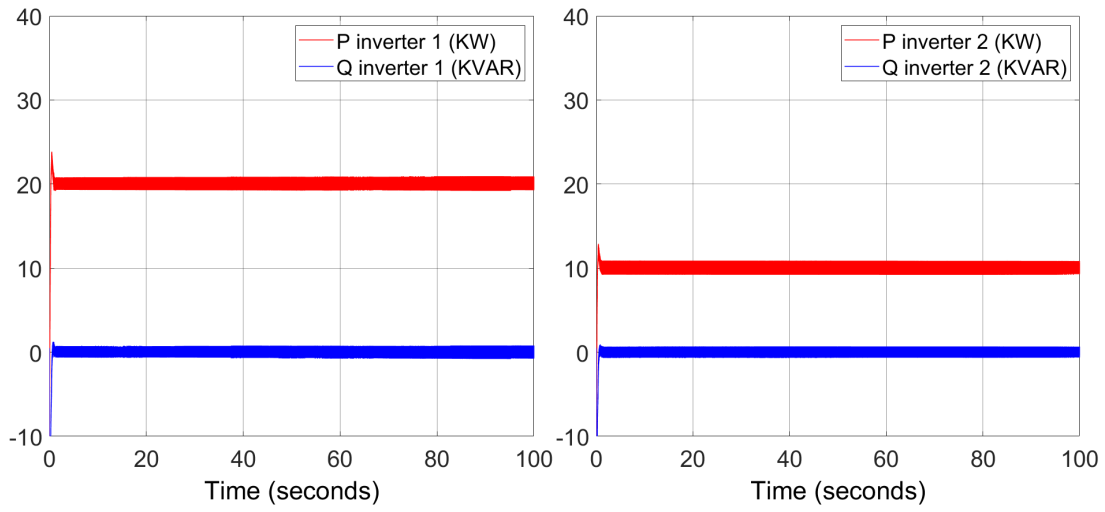


Figure 4.30: Power output of inverters in normal operation

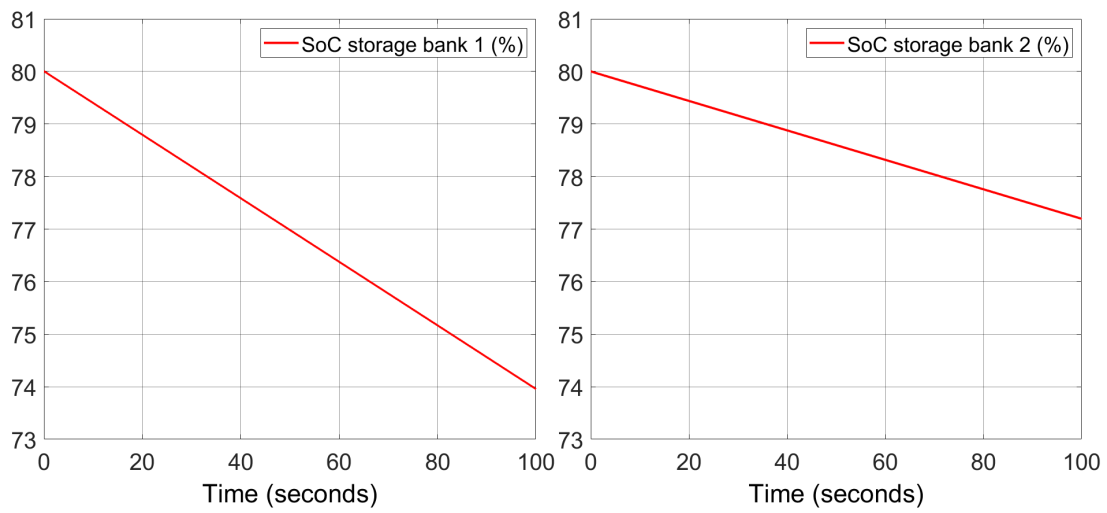


Figure 4.31: Storage banks state of charge in normal operation

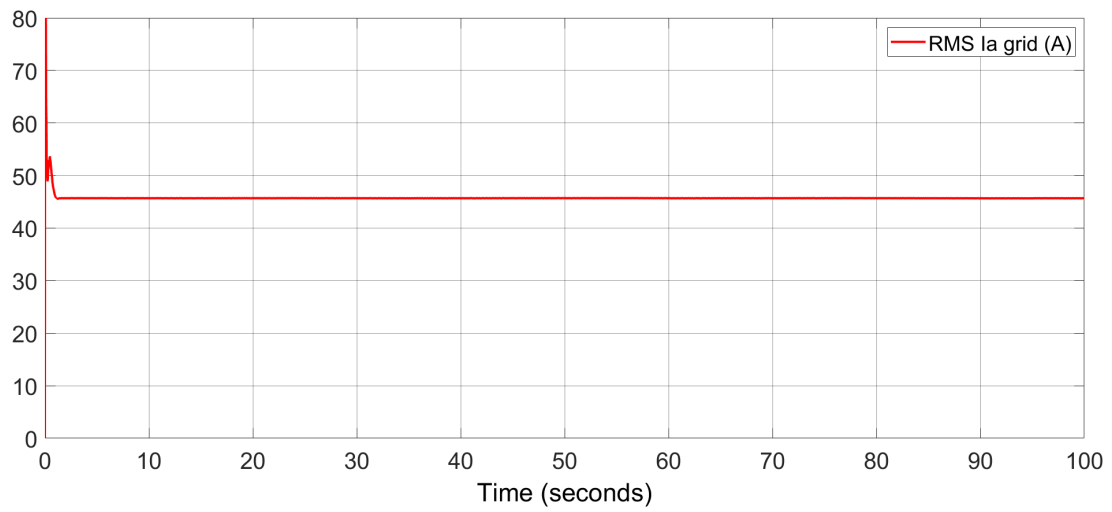


Figure 4.32: Phase 'a' RMS current injected to grid in normal operation

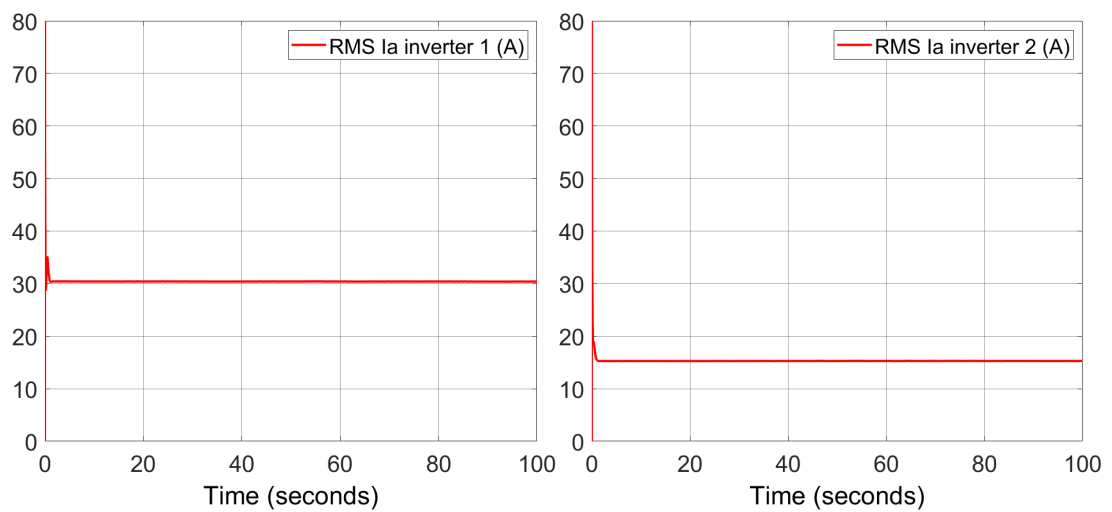


Figure 4.33: Phase 'a' RMS output currents of inverters in normal operation

4.2.1.2 Active and Reactive Power Generation

In this section, the battery banks inverters are controlled to generate active and reactive power. The power demand of inverter one is set to 20 KW and 10 KVAR whereas inverter two is set to generate 10 KW and 5 KVAR. Figures 4.34 - 4.38 show the performance of the system.

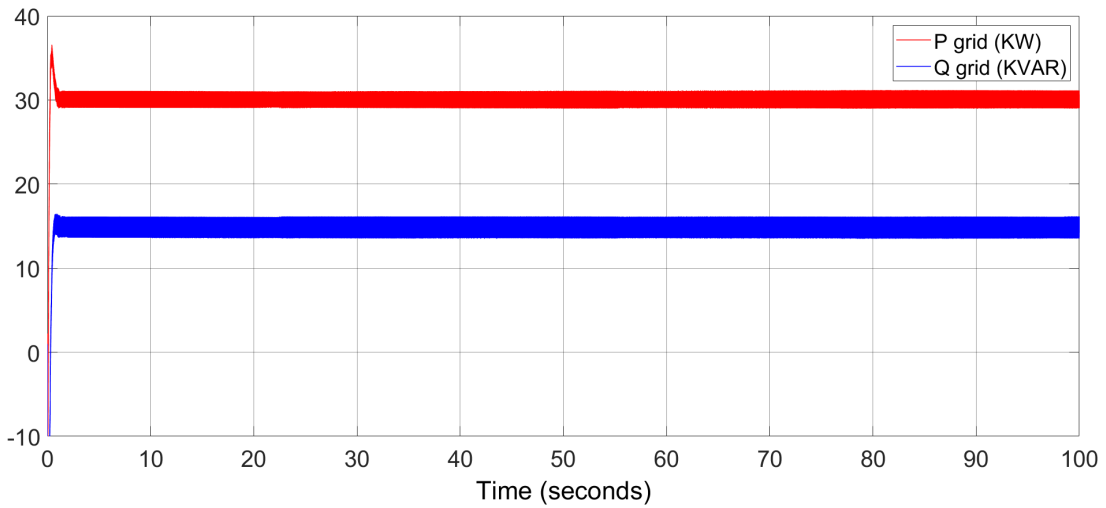


Figure 4.34: Power injected to grid in normal operation2

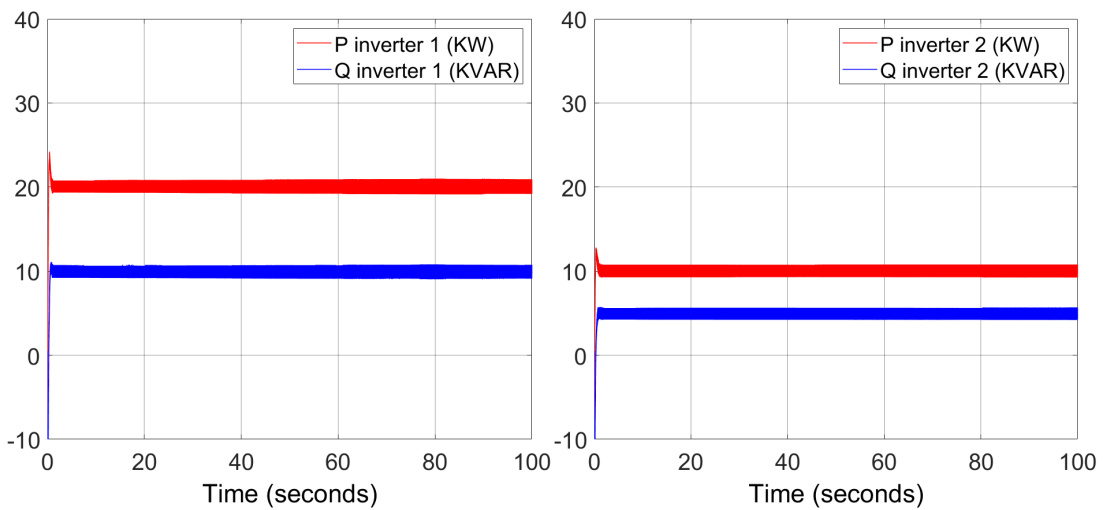


Figure 4.35: Power output of inverters in normal operation2

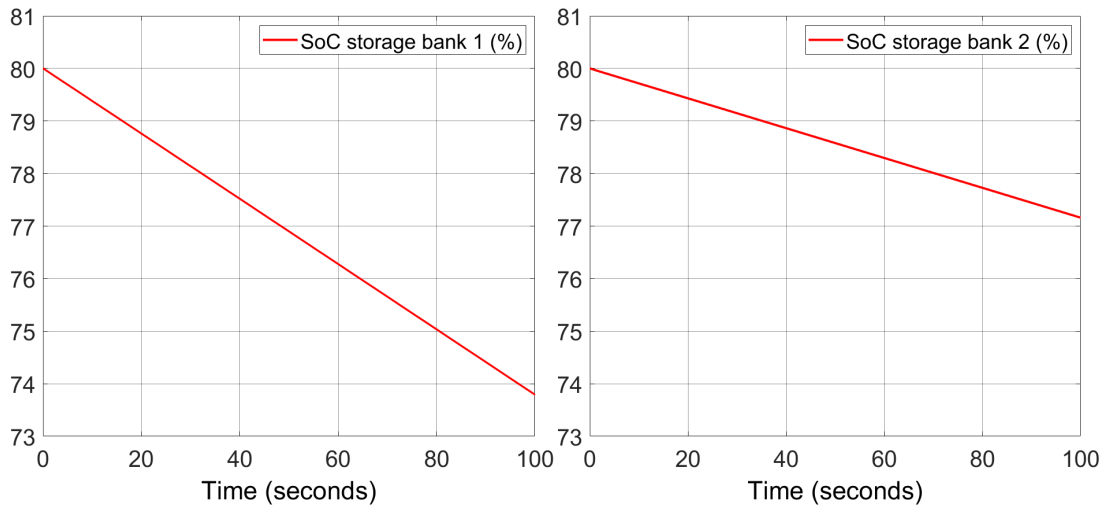


Figure 4.36: Storage banks state of charge in normal operation2

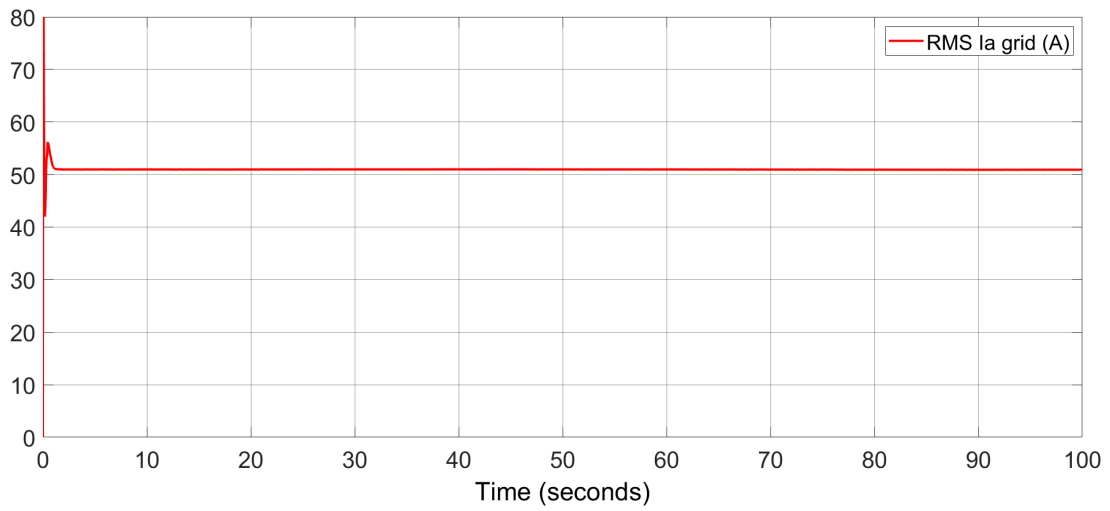


Figure 4.37: Phase 'a' RMS current injected to grid in normal operation2

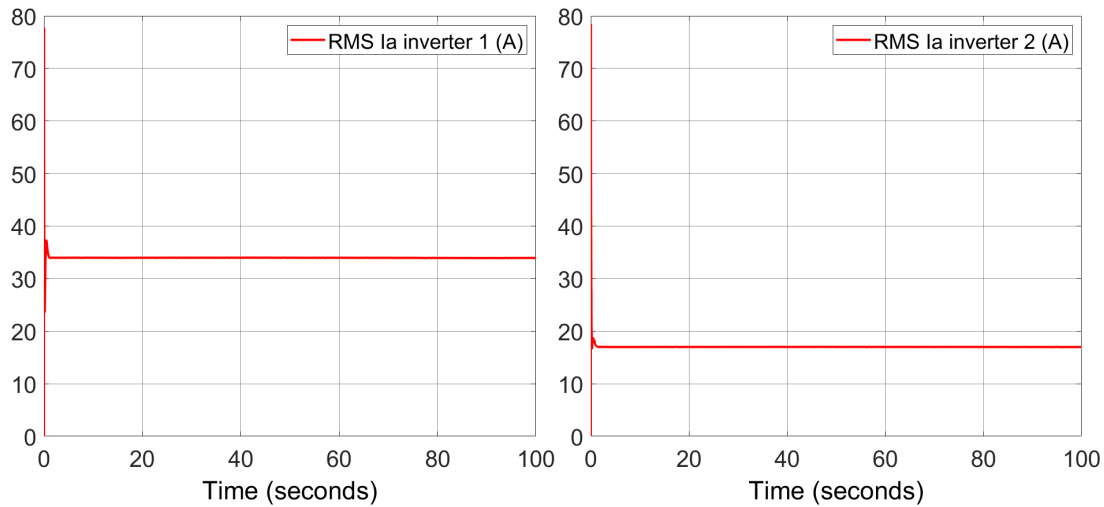


Figure 4.38: Phase 'a' RMS output currents of inverters in normal operation2

4.2.2 Fault Operation

The control of bidirectional switch follows same algorithm concerning inverters rating as in PV application.

The fault is emulated at instance $t=30s$ on inverter 2 and is isolated immediately. After 10s (at $t=40s$), the set power of the healthy inverter 1 is raised to 30 KW to compensate for the lost 10 KW as shown in Figure 4.41.

The bidirectional switch closes at $t=70s$ connecting both storage banks to the healthy inverter 1. This does not affect the power injected into the grid, but it impacts the SOC of the batteries. It is noticed from figure 4.42 that before closing the switch, the SoC of storage bank 1 was decreasing rapidly between $t=40s$ and $t=70s$. Then it returns to its normal profile after connecting the storage bank 2 in parallel. Figures 4.39 - 4.44 illustrate the performance of the system during this fault scenario.

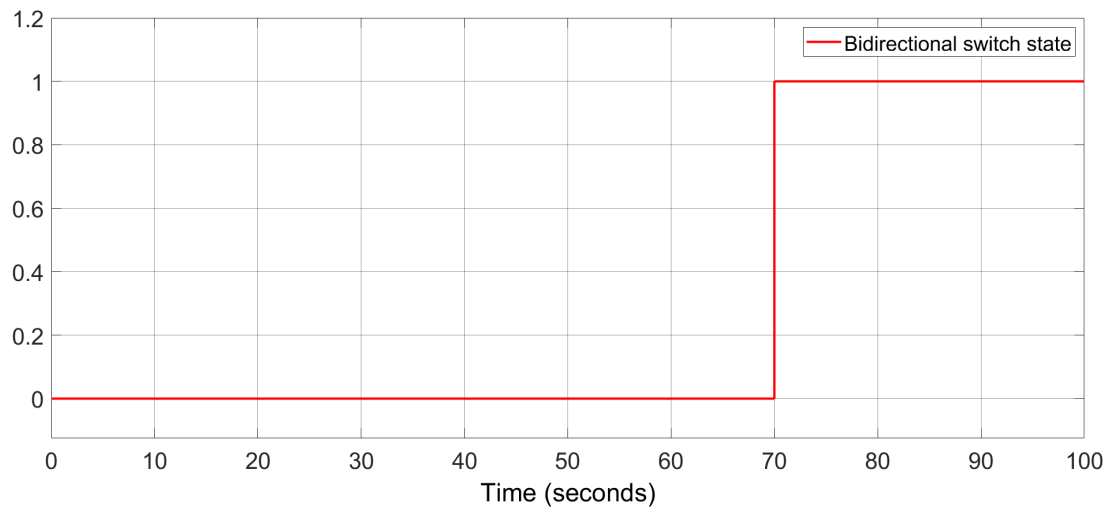


Figure 4.39: Bidirectional switch state (fault at 30s)

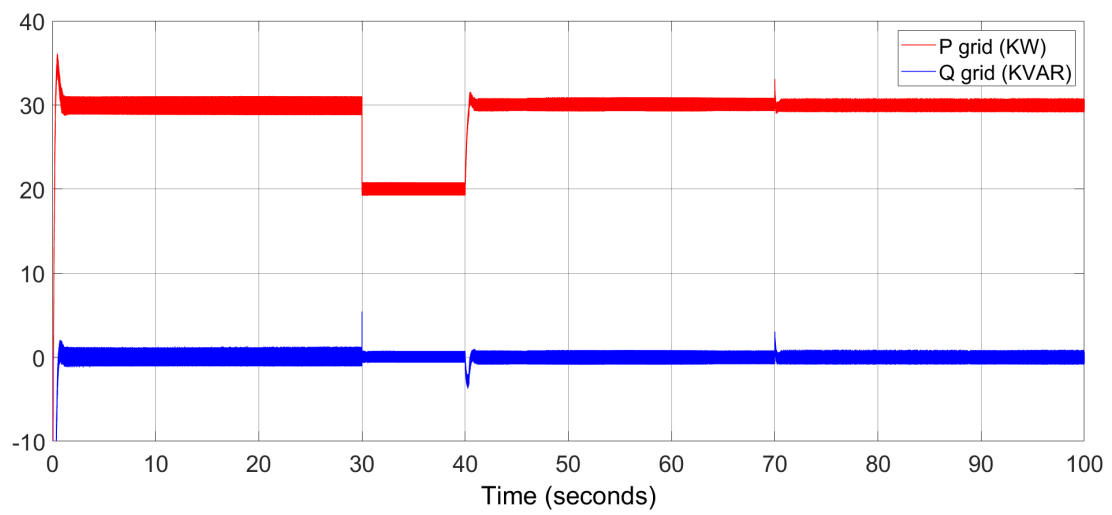


Figure 4.40: Power injected to grid (fault at 30s)

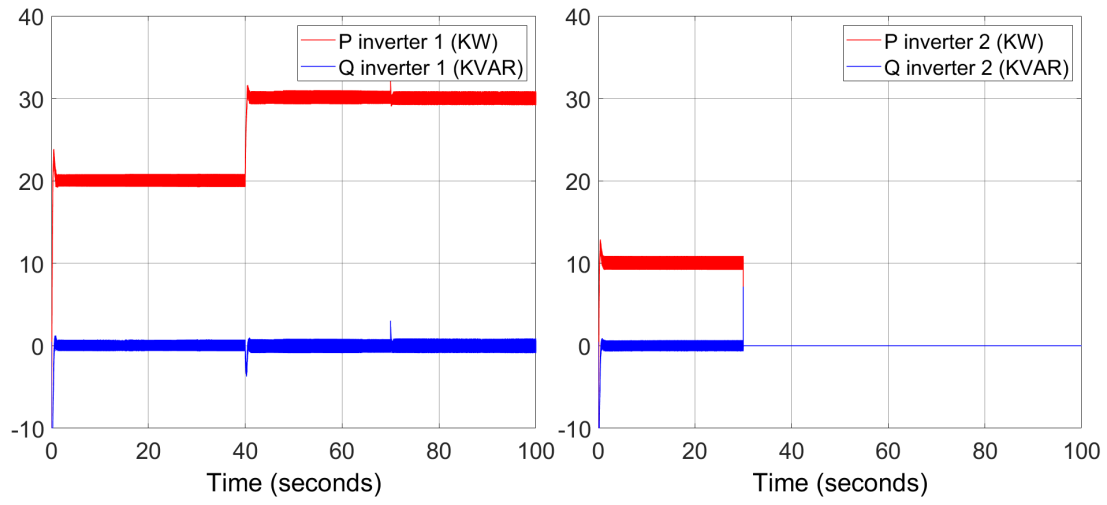


Figure 4.41: Power output of inverters 1 (healthy) and 2 (faulty) (fault at 30s)

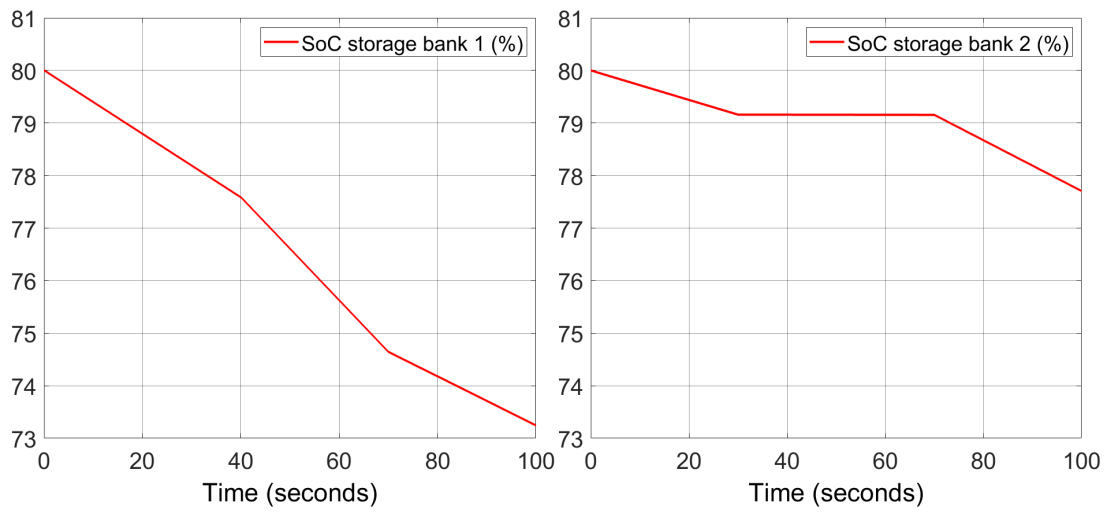


Figure 4.42: Storage banks state of charge (fault at 30s)

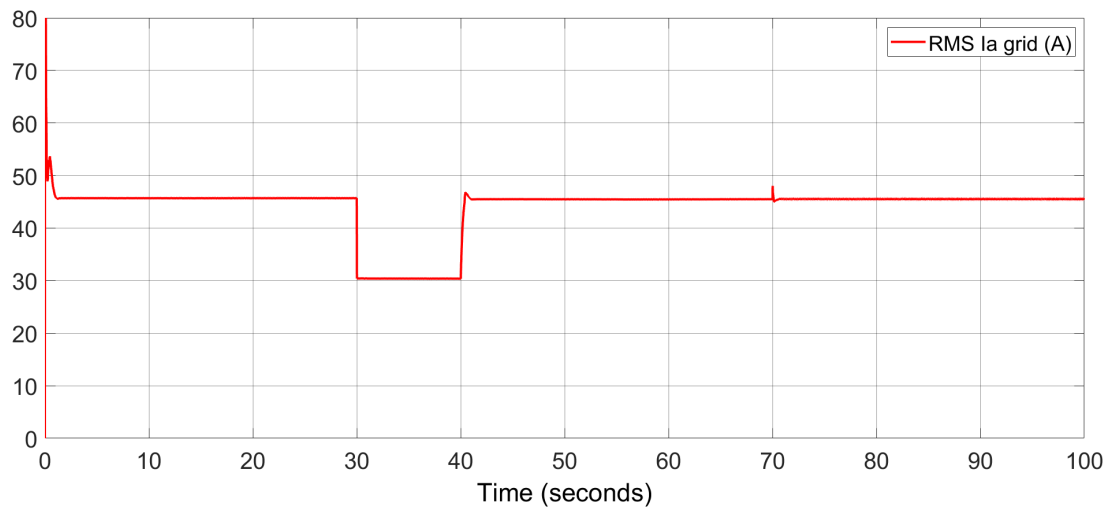


Figure 4.43: Phase 'a' RMS current injected to grid (fault at 30s)

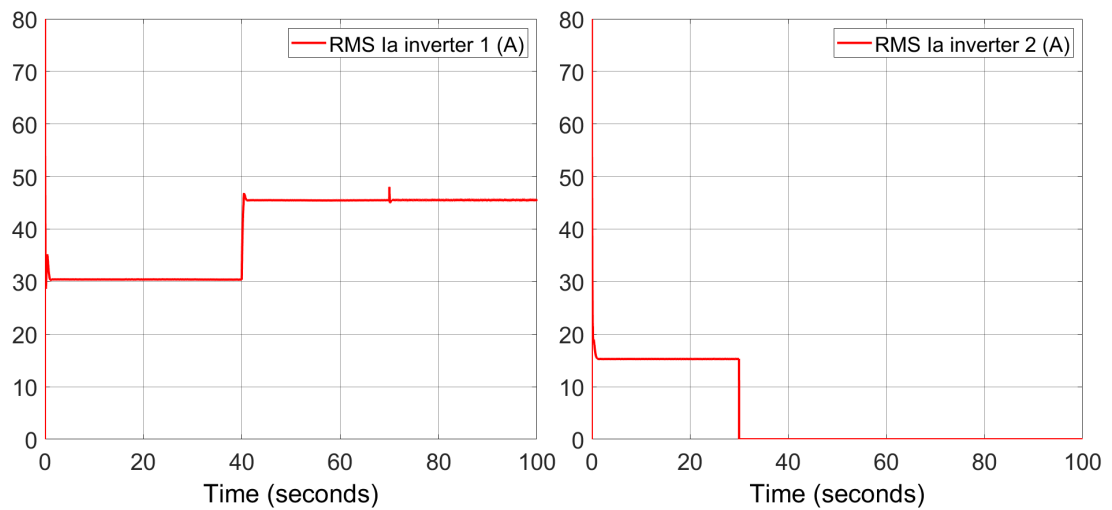


Figure 4.44: Phase 'a' RMS output currents of inverters 1 (healthy) and 2 (faulty) (fault at 30s)

4.2.3 Advantages

The first two advantages mentioned in section 4.1.3 are also valid in battery application. Besides this, the significant advantage of applying this solution on battery storage systems is that it protects the battery which is tied to the healthy inverter from rapid discharge and possible over-heating. This keeps the batteries healthy and extends its life time.

4.3 Overall Microgrid

All above above distributed generators were aggregated to form the proposed microgrid shown in figure 4.45 consisting of:

- Two solar arrays rated at 50 KW each
- Two battery banks set to supply 50 KW each
- One wind turbine rated at 500 KW
- Residential load

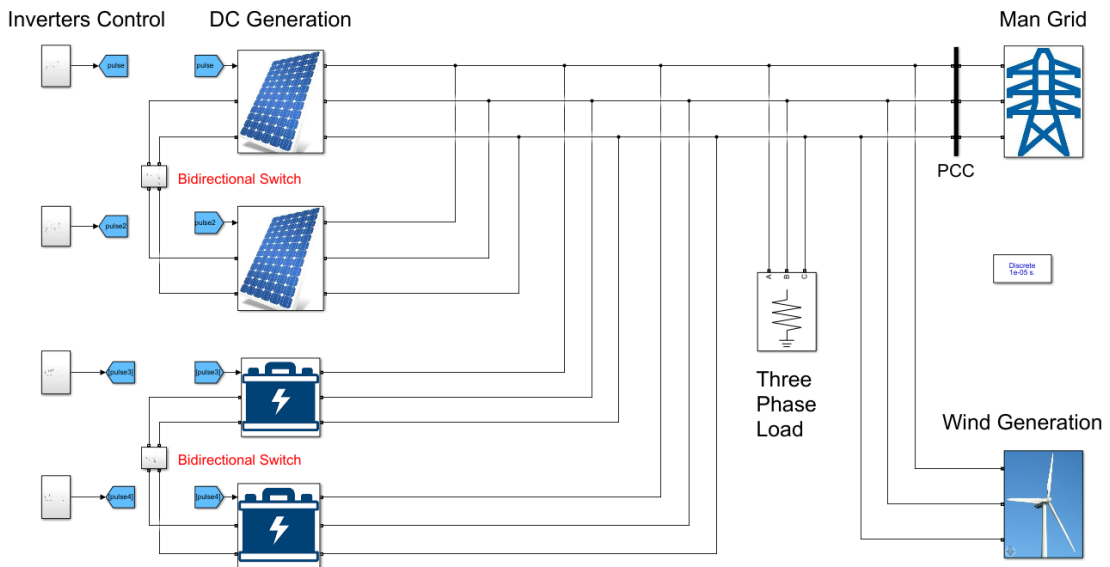


Figure 4.45: MATLAB Simulink schematic of proposed microgrid

4.3.1 Microgrid operation with no load

The microgrid is first simulated at no connected load. In this case, all the generated power (700 KW peak) is injected to the main grid as shown in figure 4.46.

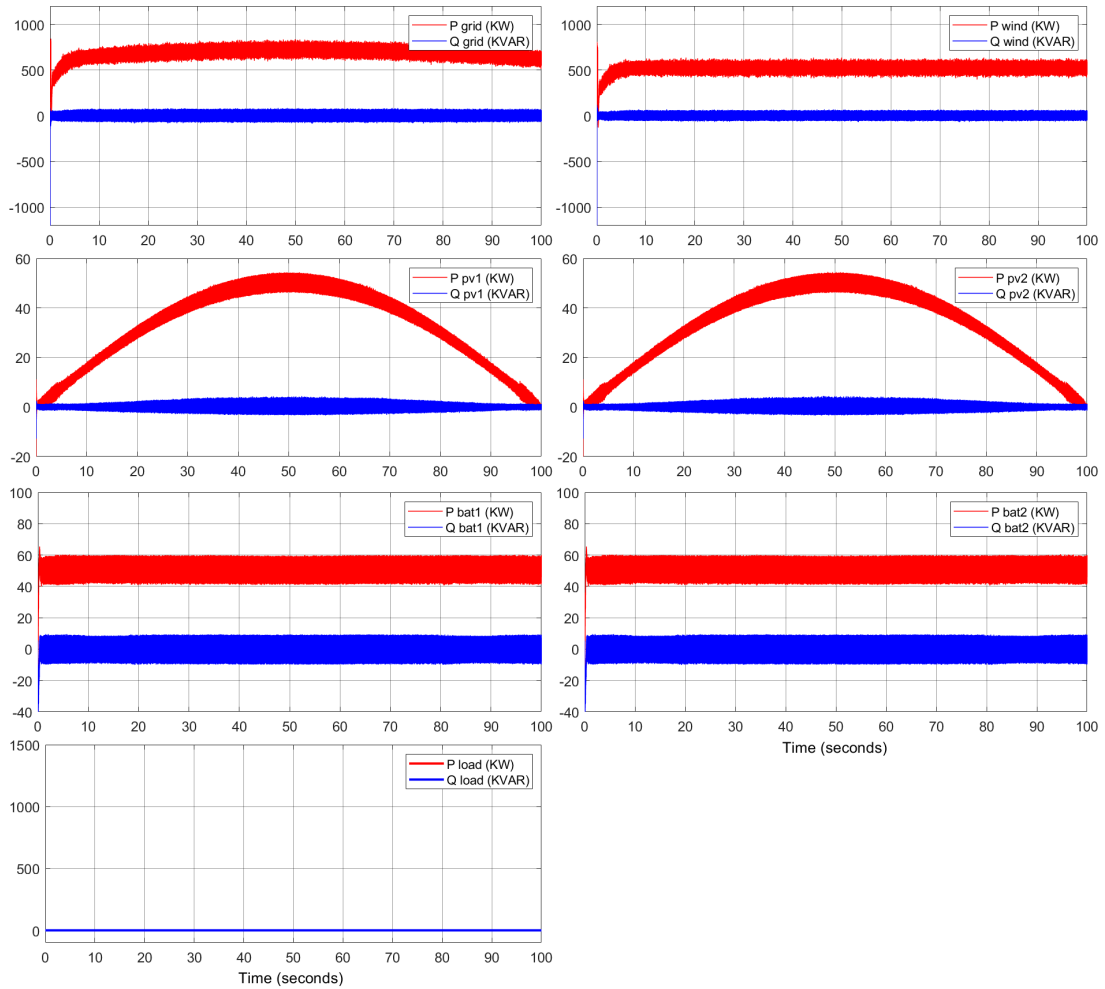


Figure 4.46: Power flow in microgrid components at no load

4.3.2 Microgrid operation with 500 KW load

A 500 KW three phase load is now connected to the microgrid. Here its noted that the power injected to main grid is reduced to around 200 KW peak as shown in figure 4.47. This is because the load is draining 500 KW of the microgrid generated power.

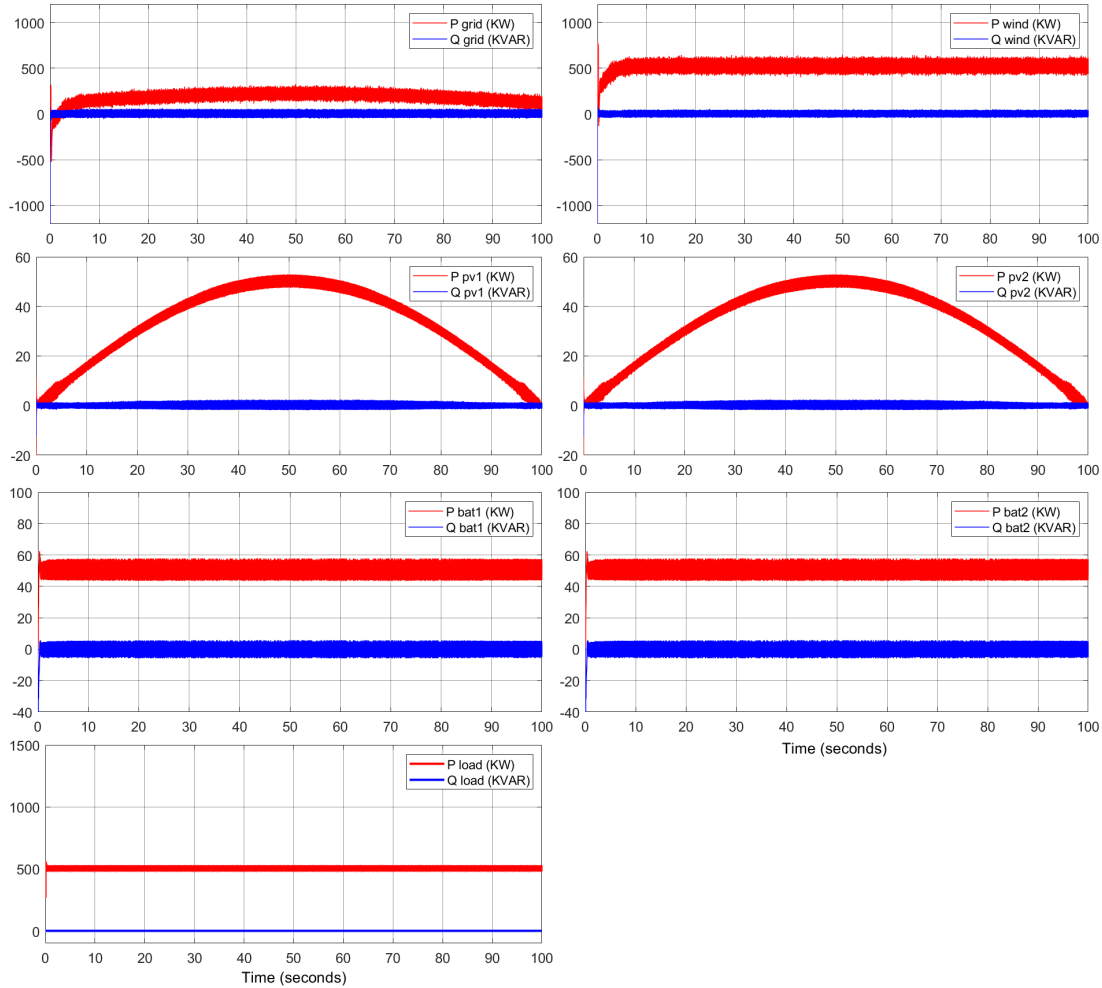


Figure 4.47: Power flow in microgrid components at 500 KW load

4.3.3 Microgrid operation with 1000 KW load

The load is increased to 1000 KW which is higher than the microgrid ability to supply. Here the latter supplies all its available power (700 KW peak) to the load and the remaining power (300 KW) is taken from the main grid. This is clear in figure 4.48 where P_{grid} becomes negative meaning that the microgrid is draining power from main grid rather than injecting.

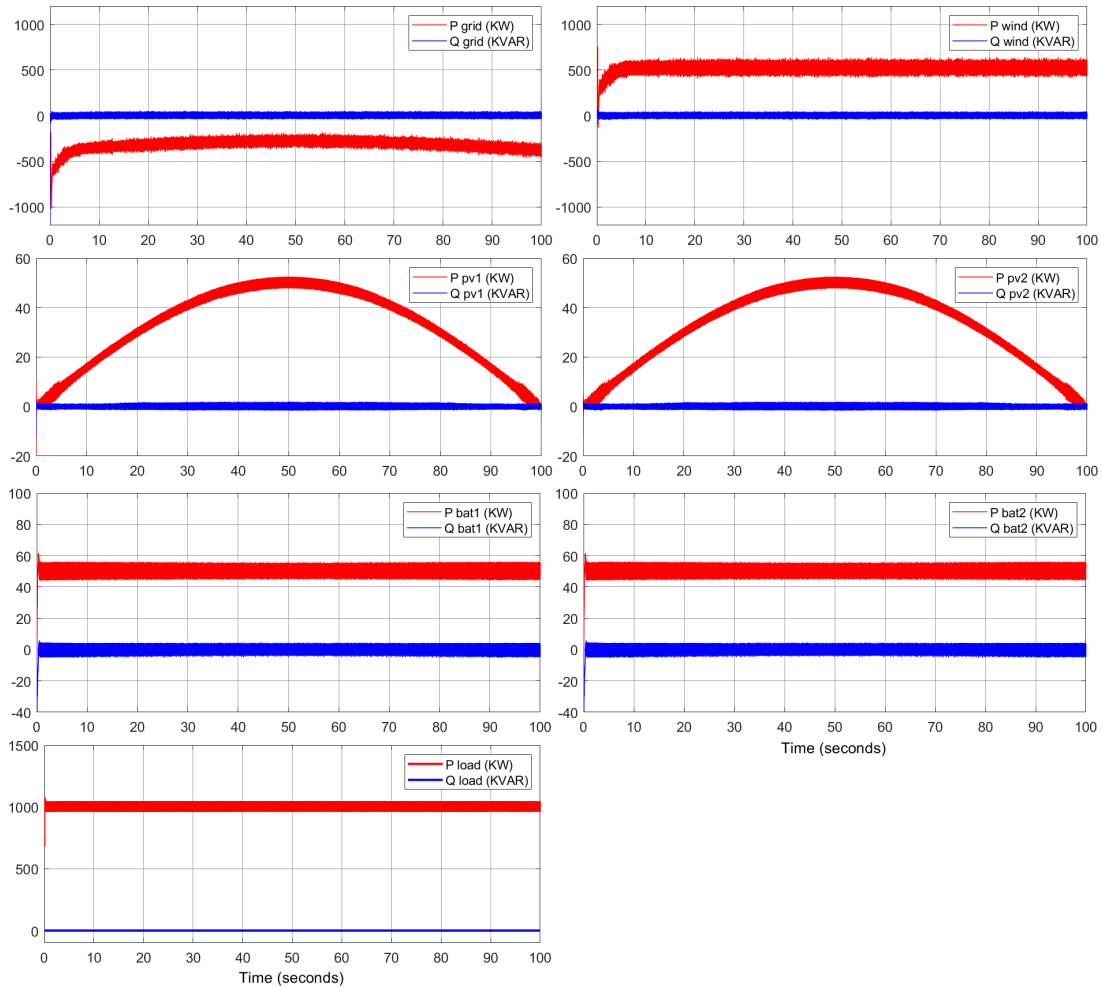


Figure 4.48: Power flow in microgrid components at 1000 KW load

4.3.4 Microgrid operation under fault with 500 KW load

The battery banks here are controlled to generate 40 KW each. Two faults were emulated on inverters connected to solar array 2 and battery bank 2. The faults occurred at $t=50s$ where P_{grid} fell down to 100 KW at peak as shown in figure 4.49. Then the algorithm worked and part of the power was retrieved.

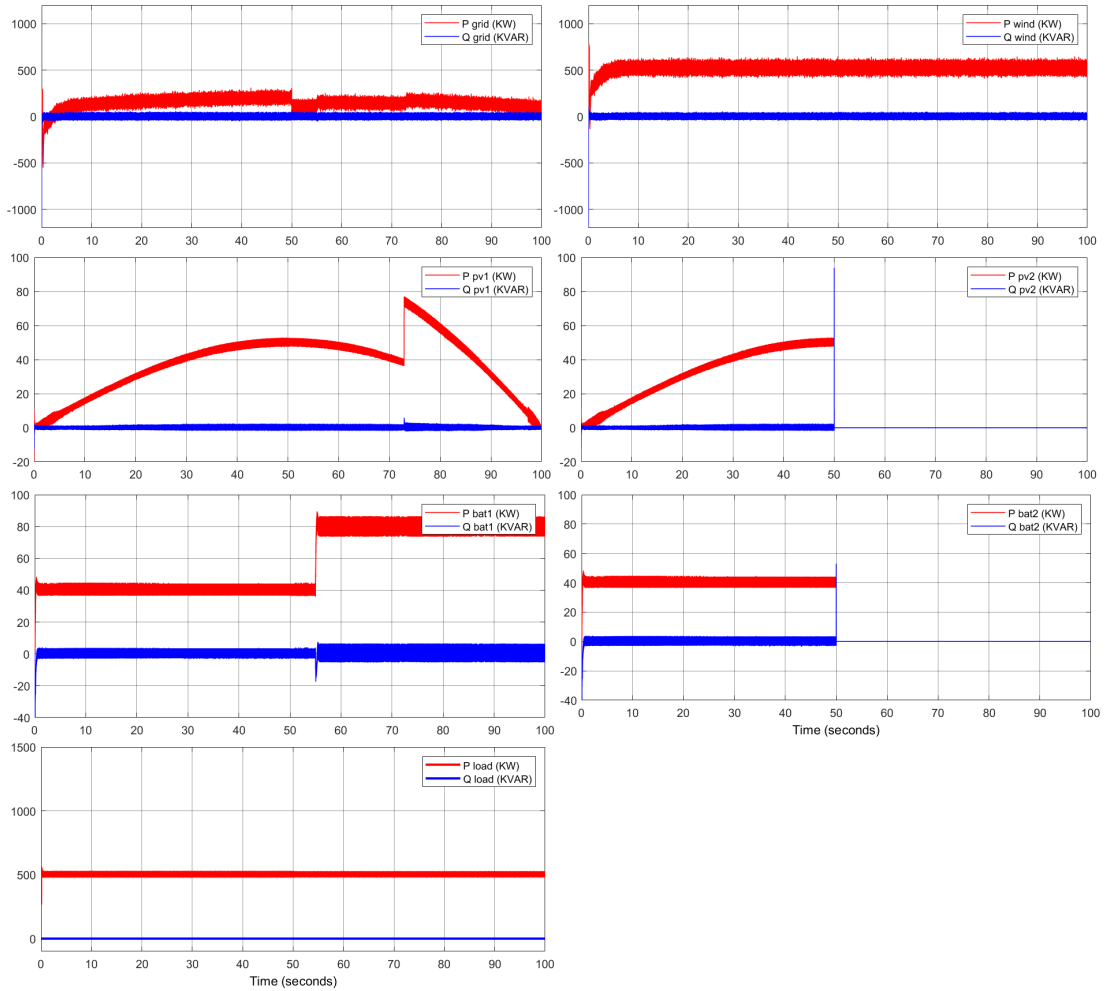


Figure 4.49: Power flow in microgrid components at 500 KW load under fault

Chapter 5

Experimental Results

The experimental setup was established at the PEARL lab [39]. Two 200Ah batteries were connected to two TDINV3500P100 inverters. The output of inverters is then rectified and connected to a common DC bus as shown in figure 5.1. A resistive load is connected at the DC bus.

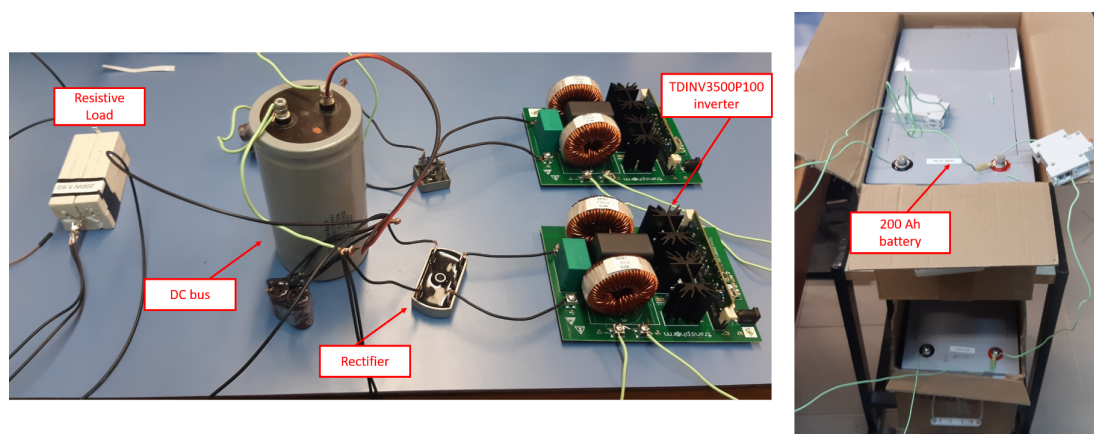


Figure 5.1: Experimental setup

The experiment started as mentioned above. At instance t_1 , inverter one was isolated due to an emulated fault. Then at instant t_2 the corresponding battery1 of isolated inverter 1 was connected in parallel with battery 2 across inverter 2. At beginning, the two batteries were sharing the load. Then after t_1 , the current drained from battery 2 increased to compensate the lost current of battery 1. Then after t_2 , the batteries share again the load. It is clear that the load voltage and current was not affected during switching and stayed constant approximately. Figures 5.2-5.4 illustrate the results.

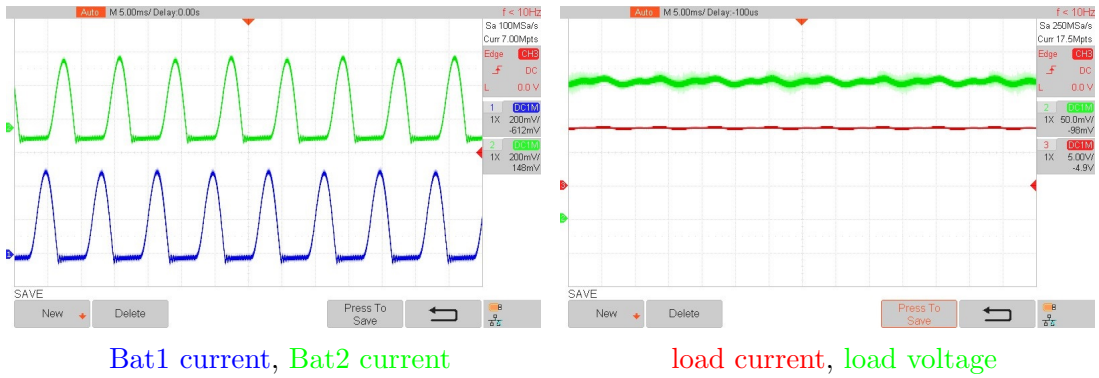


Figure 5.2: Experimental results before the fault is emulated in inverter 1

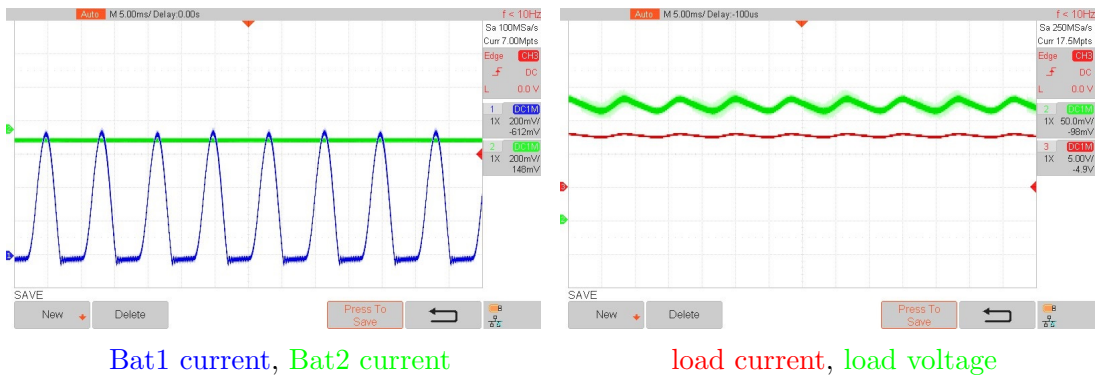


Figure 5.3: Experimental results after t_1 when inverter 1 is taken offline

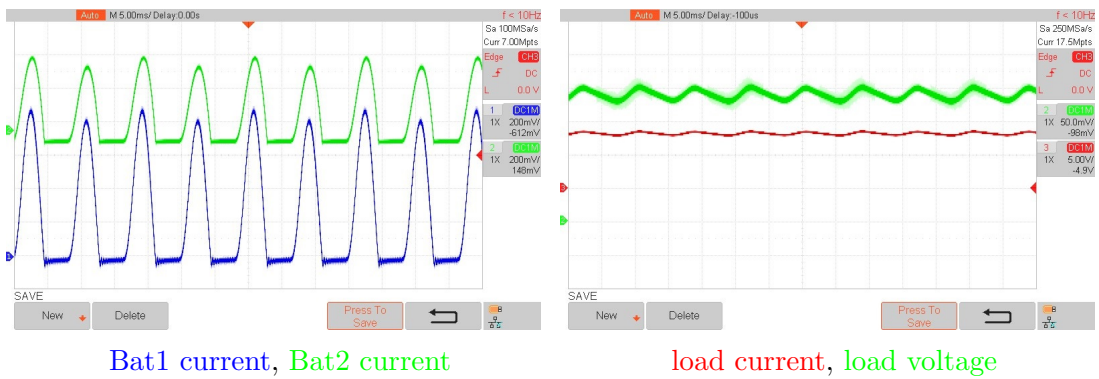


Figure 5.4: Experimental results after t_2

Chapter 6

Conclusion and Future Work

A fault-tolerant strategy to minimize curtailed power in faulty microgrid inverters is proposed in this thesis. The strategy does not require topology modification of individual inverters, or changes to their control methods. It relies on adding controlled bidirectional switches that reroute the power from faulty inverters to healthy ones in the same microgrid. Simulations were performed for two applications, PV inverters and battery inverters. Results show an increase in the harnessed energy in the PV application when compared to cutting off a faulty inverter branch. Also, a decrease in discharge rate in the battery application is illustrated, which is expected to increase a battery's life with reduced overheating that occurs with rapid discharge. An experimental prototype of the proposed method is presented. It showed the power sharing capability between batteries across the load.

For future work, this method can be extended to apply on more than two sources. Applying it between many inverters will increase the overall availability of the microgrid. This would also help retrieve more lost energy by rerouting it on several inverters rather than one. This would also necessitate a higher level controller that can command all the inverters and bidirectional switches across the microgrid. Also, the bidirectional switch can be modulated through a control scheme that specifies the amount of shared power shared through switch.

Bibliography

- [1] H. Bevrani, B. François, and T. Ise, *Microgrid dynamics and control*. John Wiley & Sons, 2017.
- [2] O. Palizban, K. Kauhaniemi, and J. M. Guerrero, “Microgrids in active network management—part i: Hierarchical control, energy storage, virtual power plants, and market participation,” *Renewable and Sustainable Energy Reviews*, vol. 36, pp. 428–439, 2014.
- [3] *CIGRE, Report on behalf of the Technical Committee. “Network of the Future”, Electricity Supply Systems of the Future, Electra, No 256*, 2011.
- [4] B. S. Pali and S. Vadhera, “Renewable energy systems for generating electric power: A review,” in *2016 IEEE 1st International Conference on Power Electronics, Intelligent Control and Energy Systems (ICPEICES)*, pp. 1–6, IEEE, 2016.
- [5] M. C. Williams, “Fuel cells and the world energy future,” in *2001 Power Engineering Society Summer Meeting. Conference Proceedings (Cat. No. 01CH37262)*, vol. 1, pp. 725–vol, IEEE, 2001.
- [6] *Department of Energy Office of Electricity Delivery and Energy Reliability Summary Report: 2012 DOE Microgrid Workshop.*, pp. 1–33, 2012.
- [7] A. Ferreira, S. S. Kunh, K. C. Fagnani, T. A. De Souza, C. Tonezer, G. R. Dos Santos, and C. H. Coimbra-Araújo, “Economic overview of the use and production of photovoltaic solar energy in brazil,” *Renewable and Sustainable Energy Reviews*, vol. 81, pp. 181–191, 2018.
- [8] Y. Song and B. Wang, “Survey on reliability of power electronic systems,” *IEEE Transactions on Power Electronics*, vol. 28, no. 1, pp. 591–604, 2012.
- [9] P. Asmus, “Microgrids, virtual power plants and our distributed energy future,” *The Electricity Journal*, vol. 23, no. 10, pp. 72–82, 2010.
- [10] H. Jiayi, J. Chuanwen, and X. Rong, “A review on distributed energy resources and microgrid,” *Renewable and Sustainable Energy Reviews*, vol. 12, no. 9, pp. 2472–2483, 2008.

- [11] Y. Zoka, H. Sasaki, N. Yorino, K. Kawahara, and C. Liu, “An interaction problem of distributed generators installed in a microgrid,” in *2004 IEEE International Conference on Electric Utility Deregulation, Restructuring and Power Technologies. Proceedings*, vol. 2, pp. 795–799, IEEE, 2004.
- [12] M. Sechilariu, B. Wang, and F. Locment, “Building integrated photovoltaic system with energy storage and smart grid communication,” *IEEE Transactions on Industrial Electronics*, vol. 60, no. 4, pp. 1607–1618, 2012.
- [13] B. H. Chowdhury, H. T. Ma, and N. Ardesna, “The challenge of operating wind power plants within a microgrid framework,” in *2010 Power and Energy Conference At Illinois (PECI)*, pp. 93–98, IEEE, 2010.
- [14] X. Wang, J. Shi, L. Liu, J. Gu, and K. Zhu, “Optimum configuration of grid-connected microgrid based on probability model,” in *2019 IEEE 8th Joint International Information Technology and Artificial Intelligence Conference (ITAIC)*, pp. 7–11, IEEE, 2019.
- [15] M. R. Sandgani and S. Sirouspour, “Energy management in a network of grid-connected microgrids/nanogrids using compromise programming,” *IEEE Transactions on Smart Grid*, vol. 9, no. 3, pp. 2180–2191, 2016.
- [16] M. Karimi, R. Azizipanah-Abarghooee, H. Uppal, Q. Hong, C. Booth, and V. Terzija, “Smart integrated adaptive centralized controller for islanded microgrids under minimized load shedding,” in *2017 5th International Istanbul Smart Grid and Cities Congress and Fair (ICSG)*, pp. 41–45, IEEE, 2017.
- [17] A. Bidram and A. Davoudi, “Hierarchical structure of microgrids control system,” *IEEE Transactions on Smart Grid*, vol. 3, no. 4, pp. 1963–1976, 2012.
- [18] O. Ahmed and J. Bleijs, “Power flow control methods for an ultracapacitor bidirectional converter in dc microgrids—a comparative study,” *Renewable and Sustainable Energy Reviews*, vol. 26, pp. 727–738, 2013.
- [19] R. Zamora and A. K. Srivastava, “Controls for microgrids with storage: Review, challenges, and research needs,” *Renewable and Sustainable Energy Reviews*, vol. 14, no. 7, pp. 2009–2018, 2010.
- [20] J. J. Justo, F. Mwasilu, J. Lee, and J.-W. Jung, “Ac-microgrids versus dc-microgrids with distributed energy resources: A review,” *Renewable and sustainable energy reviews*, vol. 24, pp. 387–405, 2013.
- [21] J. C. Vasquez, J. M. Guerrero, J. Miret, M. Castilla, and L. G. De Vicuna, “Hierarchical control of intelligent microgrids,” *IEEE Industrial Electronics Magazine*, vol. 4, no. 4, pp. 23–29, 2010.

- [22] L.-J. Qin and W.-T. Yang, “Micro-grid converter droop control strategy and simulation,” in *Advances in Electrical and Computer Engineering*, pp. 74–80.
- [23] J. M. Guerrero, J. C. Vasquez, J. Matas, L. G. De Vicuña, and M. Castilla, “Hierarchical control of droop-controlled ac and dc microgrids—a general approach toward standardization,” *IEEE Transactions on industrial electronics*, vol. 58, no. 1, pp. 158–172, 2010.
- [24] Q.-T. An, L.-Z. Sun, K. Zhao, and L. Sun, “Switching function model-based fast-diagnostic method of open-switch faults in inverters without sensors,” *IEEE Transactions on Power Electronics*, vol. 26, no. 1, pp. 119–126, 2010.
- [25] J. Hare, X. Shi, S. Gupta, and A. Bazzi, “Fault diagnostics in smart micro-grids: A survey,” *Renewable and Sustainable Energy Reviews*, vol. 60, pp. 1114–1124, 2016.
- [26] W. Chen, E. Hotchkiss, C. Mademlis, and A. M. Bazzi, “Integrated fault diagnosis and recovery in npc multi-level inverters,” in *2017 IEEE 11th International Symposium on Diagnostics for Electrical Machines, Power Electronics and Drives (SDEMPED)*, pp. 415–421, IEEE, 2017.
- [27] W. Zhang, D. Xu, P. N. Enjeti, H. Li, J. T. Hawke, and H. S. Krishnamoorthy, “Survey on fault-tolerant techniques for power electronic converters,” *IEEE Transactions on Power Electronics*, vol. 29, no. 12, pp. 6319–6331, 2014.
- [28] J. Andreu, I. Kortabarria, E. Ibarra, I. M. de Alegría, and E. Robles, “A new hardware solution for a fault tolerant matrix converter,” in *2009 35th Annual Conference of IEEE Industrial Electronics*, pp. 4469–4474, IEEE, 2009.
- [29] A. L. Julian and G. Oriti, “A comparison of redundant inverter topologies to improve voltage source inverter reliability,” *IEEE Transactions on Industry Applications*, vol. 43, no. 5, pp. 1371–1378, 2007.
- [30] Z. Yi, S. Hongge, and X. Bin, “Optimization of neutral shift in cell-fault treatment for cascaded h-bridge inverter,” in *2008 International Conference on Electrical Machines and Systems*, pp. 1683–1685, IEEE, 2008.
- [31] W. Song and A. Q. Huang, “Fault-tolerant design and control strategy for cascaded h-bridge multilevel converter-based statcom,” *IEEE Transactions on Industrial Electronics*, vol. 57, no. 8, pp. 2700–2708, 2009.
- [32] J. M. Guerrero, J. C. Vasquez, J. Matas, M. Castilla, and L. G. de Vicuña, “Control strategy for flexible microgrid based on parallel line-interactive ups systems,” *IEEE Transactions on industrial Electronics*, vol. 56, no. 3, pp. 726–736, 2008.

- [33] Z. Ye, D. Boroyevich, J.-Y. Choi, and F. C. Lee, “Control of circulating current in two parallel three-phase boost rectifiers,” *IEEE Transactions on power electronics*, vol. 17, no. 5, pp. 609–615, 2002.
- [34] C. Arbugeri, N. Pont, T. Jappe, S. Mussa, and T. Lazzarin, “Control system for multi-inverter parallel operation in uninterruptible power systems,” *Eletrônica de Potência*, vol. 24, pp. 1–11, 02 2018.
- [35] X. Sun, L.-K. Wong, Y.-S. Lee, and D. Xu, “Design and analysis of an optimal controller for parallel multi-inverter systems,” *IEEE Transactions on Circuits and Systems II: Express Briefs*, vol. 53, no. 1, pp. 56–61, 2006.
- [36] A. Akhavan, H. R. Mohammadi, and J. M. Guerrero, “Modeling and design of a multivariable control system for multi-paralleled grid-connected inverters with lcl filter,” *International Journal of Electrical Power & Energy Systems*, vol. 94, pp. 354–362, 2018.
- [37] L. Asiminoaei, E. Aeloiza, P. N. Enjeti, and F. Blaabjerg, “Shunt active-power-filter topology based on parallel interleaved inverters,” *IEEE Transactions on Industrial Electronics*, vol. 55, no. 3, pp. 1175–1189, 2008.
- [38] https://re.jrc.ec.europa.eu/pvg_tools/en/DR.
- [39] <https://sites.aub.edu.lb/pearl/>.

